University of Tennessee, Knoxville
TRACE: Tennessee Research and Creative Exchange

Masters Theses | Graduate School

5-2021

APPLICATION OF TITRATIONS FOR VERIFICATION OF SMALL MOLECULE INTERACTION IN RELATION TO AMIDOXIMATED FIBERS FOR URANIUM EXTRACTION FROM SEAWATER

Kc Michael Mote
University of Tennessee, Knoxville, kgreenup@vols.utk.edu

Follow this and additional works at: https://trace.tennessee.edu/utk_gradthes

 Part of the Environmental Chemistry Commons, Inorganic Chemistry Commons, Materials Chemistry Commons, and the Oil, Gas, and Energy Commons

Recommended Citation

Mote, Kc Michael, "APPLICATION OF TITRATIONS FOR VERIFICATION OF SMALL MOLECULE INTERACTION IN RELATION TO AMIDOXIMATED FIBERS FOR URANIUM EXTRACTION FROM SEAWATER. " Master's Thesis, University of Tennessee, 2021.
https://trace.tennessee.edu/utk_gradthes/6218

This Thesis is brought to you for free and open access by the Graduate School at TRACE: Tennessee Research and Creative Exchange. It has been accepted for inclusion in Masters Theses by an authorized administrator of TRACE: Tennessee Research and Creative Exchange. For more information, please contact trace@utk.edu.

To the Graduate Council:

I am submitting herewith a thesis written by Kc Michael Mote entitled "APPLICATION OF TITRATIONS FOR VERIFICATION OF SMALL MOLECULE INTERACTION IN RELATION TO AMIDOXIMATED FIBERS FOR URANIUM EXTRACTION FROM SEAWATER." I have examined the final electronic copy of this thesis for form and content and recommend that it be accepted in partial fulfillment of the requirements for the degree of Master of Science, with a major in Chemistry.

Sheng, Dai, Major Professor

We have read this thesis and recommend its acceptance:

Craig E. Barnes, Shawn R. Campagna

Accepted for the Council:
Dixie L. Thompson

Vice Provost and Dean of the Graduate School

(Original signatures are on file with official student records.)

APPLICATION OF TITRATIONS FOR VERIFICATION OF SMALL MOLECULE INTERACTION IN RELATION TO AMIDOXIMATED FIBERS FOR URANIUM EXTRACTION FROM SEAWATER

A Thesis Presented for the
Master of Science
Degree
The University of Tennessee, Knoxville

KC Michael Mote
May 2021

Copyright © 2021 by KC Michael Mote.
All rights reserved.

ABSTRACT

Nuclear energy is a promising substitute for fossil fuels due to possessing low carbon emissions and providing scalable base-load power. However, one major drawback of using nuclear fuel as an energy source is that it needs a steady source of uranium. While the most economical method of obtaining uranium is through conventional terrestrial mining of the ore uranite, mining uranium ores is both harmful to the environment and limited by the terrestrial uranium supply, which is estimated at only 100 more years[1]. There is roughly 4,000 million tons of uranium dissolved in seawater which is magnitudes more than is in terrestrial ores. Having the ability to economically extract uranium (and other critical metals) from this unconventional reserve would ensure uranium fuel security. Although there has been a plethora of research conducted on small molecules, polymers, and fibers that can selectively bind significant amounts of uranium from aqueous media, the extraction of uranium from seawater is still not economically competitive with terrestrial extraction methods. In this research, complexometric titrations have been performed on computationally predicted and rationally designed methylated amidoxime derivatives to quantify the affinity and binding strengths of small molecule analogues to validate and improve computationally-based design principles.

TABLE OF CONTENTS

LIST OF TABLES

LIST OF FIGURES

LIST OF SCHEMES

CHAPTER ONE

INTRODUCTION AND GENERAL INFORMATION

Introduction

The growing demand for electricity is driven by an increasing global population coupled with rapid industrialization in emerging economies and commensurate improvements in standard of living. While fossil fuel-based power production schemes have been the foundation for all previous development, the unchecked release of CO_2, soot, NO_2, and other pollutants has damaging effects on public health as well as both local and global ecologies. As a result, there is a burgeoning global demand for clean energy resources capable of replacing fossil fuel-based technologies for baseload power delivery. Among currently available alternative energy sources, nuclear has proven to be both more practical and economical due to its long lifetime, low carbon emission, and broad implementation.

However, one challenge for long term use of nuclear power for energy production is the need for a steady supply of uranium. Currently the most economical method of obtaining uranium is through terrestrial mining. However, as expected mining uranium ores is harmful to the environment.[2] It is estimated that there is currently 4.5 billion tons of uranium in seawater[3, 4] which can potentially be used as a cleaner nuclear fuel source. The primary challenges of sequestering uranium from seawater are that the uranium concentration in seawater is very low,

(3.3) ppb,[3, 5] and there are numerous metal cations competing with uranyl that are present at much higher concentrations[6-9]. The challenge of engineering and screening small molecule analogs that can accurately represent the deployed adsorbent has yet to be overcome.

CHAPTER TWO

LITERATURE REVIEW AND METHOD BACKGROUND

Literature Review

There have been numerous efforts to extract uranium from seawater.[5, 10-12] Currently the extraction of uranium from seawater is not economically competitive with terrestrial extraction methods.[13-15] This research focuses on using complexometric, potentiometric, and spectroscopic titration as methods to screen small molecule analogs and rationally designed ligands before they are grafted onto fibers[16-18] for deployment in seawater.

Initial adsorbent studies focused largely on inorganic adsorbents and liquid-liquid extraction, before transitioning to organo-functionalized resins in the late 1970's and early 1980's.[13] One major breakthrough was the discovery that amidoxime binds uranium with high affinity and selectivity.[11, 12, 15] The next major development was by Tamada and colleagues, who developed amidoxime-functionalized polymers, which could be deployed in the open ocean as braided adsorbents and extract up to 1.5 mg of U / g adsorbent over 30 days[5, 10]. The report was the first to identify amidoximes as a promising functionality for uranium recovery from seawater. Such work clearly establishes proof-of-concept and demonstrates the potential for the recovery of uranium from seawater at an industrial scale (Figure 1)[3, 4, 12, 19, 20].

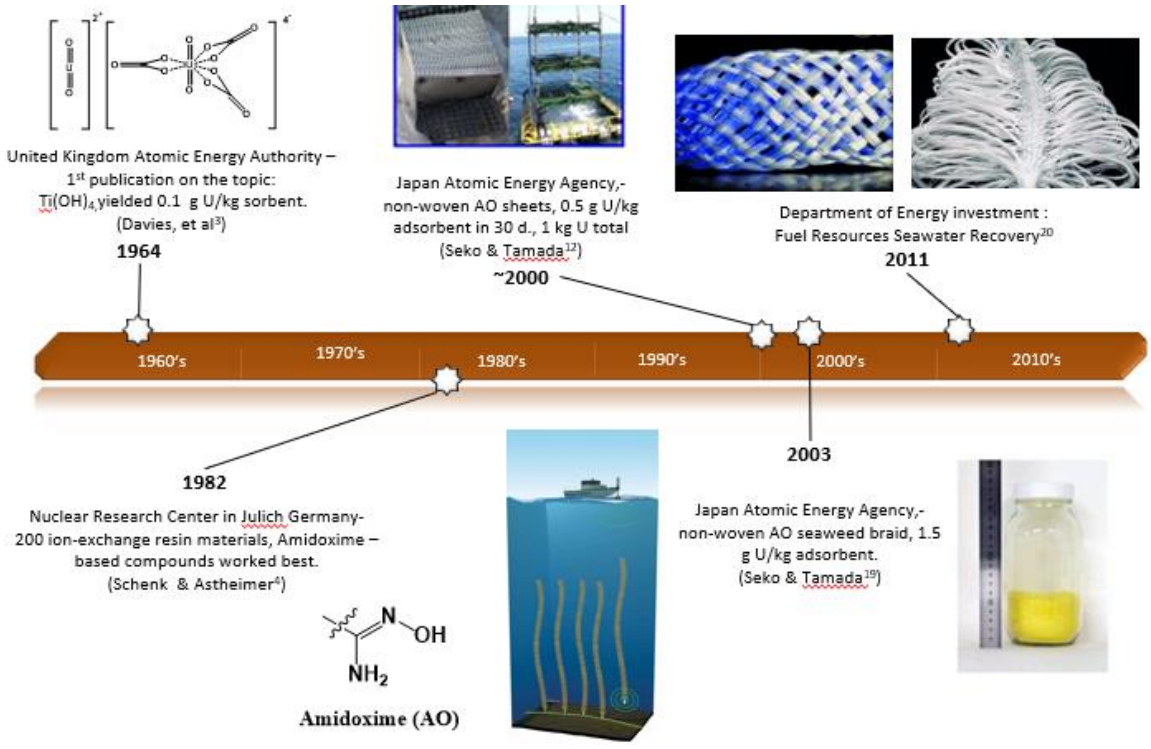

Figure 1: Progress made towards amidoxime-functionalized polymers for the adsorption of uranium from seawater.

Although it is known amidoxime-functionalized adsorbents concentrate uranium dramatically, further improvements in performance require definitive understanding of how uranium (VI) dioxide, referred to as uranyl, is coordinated by the amidoxime functionality. Astheimer et al purported that a cyclic imidedioxime functionality, formed as a byproduct of amidoximation is what is actually the moiety coordinating the uranium.[11] Supporting this claim, titrations performed by Tian et al showed two open-chain amidoximes bind less strongly than cyclic imidedioxime.[21] Titrations revealing the binding strength for several competing metals with the cyclic imidedioxime[22] have also been reported. Potentiometric titrations have been performed using a small molecule analogue representative of the cyclic imidedoxime coordinating site, and it was determined that while uranium is bound very strongly,[23] vanadyl (VO^{2+}) is bound even more strongly than uranium by the cyclic imidedioxime.[24] Nevertheless, a small molecule NMR study regarding the formation of the cyclic imidedioxmes[25] was done to aid cyclic imidedioxime formation on future adsorbents.[26] While modest improvements in uranium uptake were reported by this approach, confirmation of the binding site has not been achieved. Furthermore, preparation of an engineered cyclic imidedioxime receptor, grafted onto a polymer trunk did not work as well as was anticipated.[27]

Computationally-guided design of uranyl chelator was reported by Vukovic[28] and his team that purposed a method for computationally predicting chelators that would have strong bonding and selectivity towards uranium, assuming an η^2 binding mode is achieved, as predicted for binding of uranyl by

non-cyclic amidoximes (Figure 2).[29, 30] Computationally predicted pre-organized uranyl receptors were titrated by Mehio[17, 18, 31] Lashley[16] and showed promise in terms of bond strength, however, they did not perform well when grafted onto a polymer support.

There are noteworthy differences between the small molecule and polymers protonation constants, known as pK_a's determined through complexometric titrations and potentiometric titrations, respectively. These differences in pK_a's are indicative of different binding strength, and potentially different biding modes between the small molecules and the polymers.

Benzamidizolepyridine (BIP) was designed by Dr. J. Casey Johnson as a computationally predicted and rationally designed ligand for complexometric titration studies (Figure 3). BIP was chosen for this research because of size exclusion; it has been suggested by Rowans[32, 33] group that uranyl is a better fit than smaller transition metals. In determining the binding constants of BIP in solution and comparing the results with those of BIP and copper, BIP and iron, BIP and nickel, BIP and uranium, and BIP and zinc, will give a greater understanding of the chemistry occurring at the molecular level and will be able to determine if this improved molecular understanding can be used to predict bulk adsorbent performance for uranium uptake and selectivity.

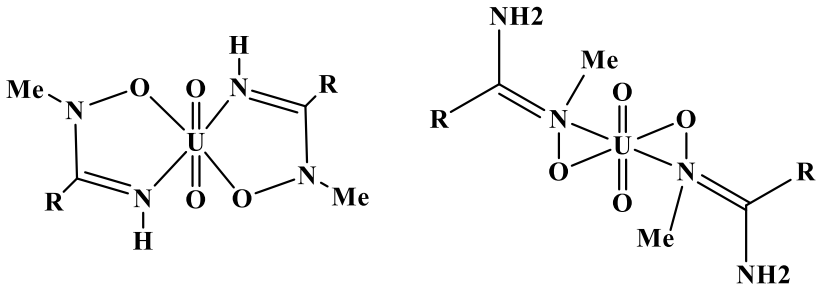

Figure 2: Schematic representation of Compound #2 bound to uranyl, (Left) κ^2 (chelating) coordination, (Right) η^2 binding mode that is not possible with the addition of the methyl group.

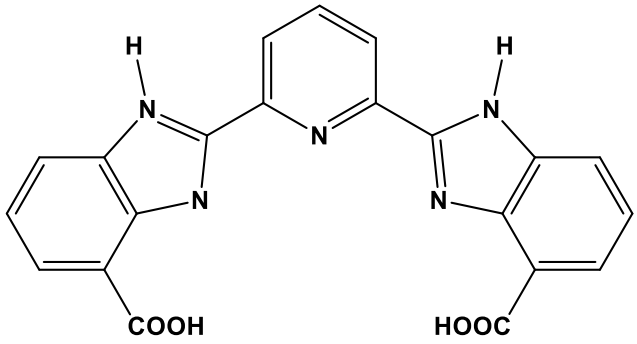

Figure 3: Structure of Bis(benzimidazolyl)pyridine, BIP.

Work done by Abney[34, 35] et al indicates small molecule analogues possess different extended x-ray absorption fine structure (EXAFS) spectra than adsorbents contacted with uranium in a brine solution, while seawater-contacted adsorbents possess even more divergent spectra, suggestive of an adjacent transition metal in the uranium binding environment. Two theories could explain this observed discrepancy. The first is that amidoximation by-products are the moiety's coordinating the uranyl, not the amidoxime itself. This is supported by the observation that < 1% of all putative U-binding sites are occupied upon adsorbent saturation, therefore numerous reaction by-products are theoretically possible. By looking at the adsorption preparation the possible by-products can be predicted. The adsorbent preparation is done by Radiation-Induced Graft Polymerization (RIGP) technology (Figure 4)[20, 35, 36]. The polymer is irradiated by an electron beam and forms reactive free radicals throughout the volume of the polyethylene fiber, then the monomers are grafted onto the polymer fiber through the polymerization of acrylonitrile and hydrophilic methacrylic acid and the adsorbent swells. After the swelling of the adsorbent functional group conversion is done using hydroxylamine and MeOH:H_2O (50:50) to form amidoxime functional groups. The adsorbent is then conditioned with potassium hydroxide (2.5 wt%) swelling the adsorbent and converting some adjacent amidoxime groups to imideoxime (cyclic form) and carboxylate groups.

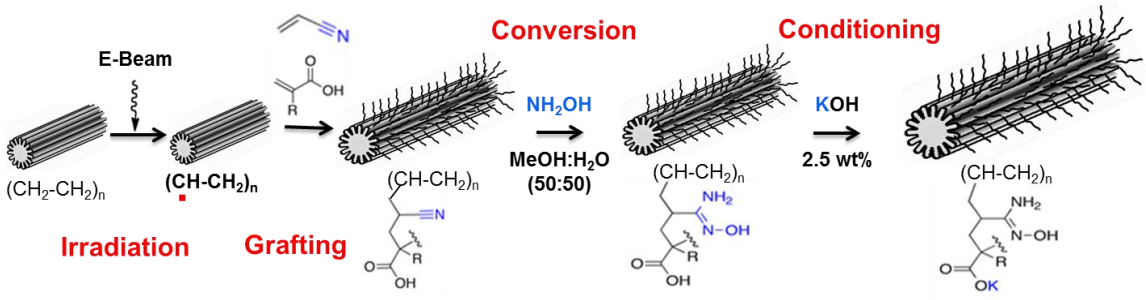

Figure 4: Adsorbent preparation by Radiation-Induced Graft Polymerization (RIGP) technology.

The amidoxime based uranium adsorbents are a complex system of interconverting ligating groups that are difficult to characterize and cannot be investigated directly and little work has been done to characterize the polymer itself after amidoximation and KOH conditioning. The functional groups that can be present on the fiber after hydroxylamine and base treatment are presented in Figure 5[20, 37-40]. The second theory that could explain this phenomena is that the morphology of the adsorbent influences the uranium binding mode, which is supported by the alleged transition metal adjacent to the uranium for the EXAFS work and that distinctly different spectra were obtained for adsorbent samples contacted in seawater and brine[34, 35].

To resolve this controversy amidoxime derived small molecules have been designed to act as proxies for existing fibers. Methylated amidoximes, with the methyl-group on the oxime nitrogen, are expected to force the κ^2 (chelating) coordination motif as is proposed from EXAFS studies[34, 35]. The oxime-methyl group will disrupt the structure such that the η^2 -coordination motif observed in single crystal studies is no longer possible. By investigating this series of methylated amidoxime derivatives (Figure 6) and obtaining the binding constants of Compounds 2 and 3 through complexometric titrations, in the future researchers will be able to rationally test the EXAFS-proposed binding mode.

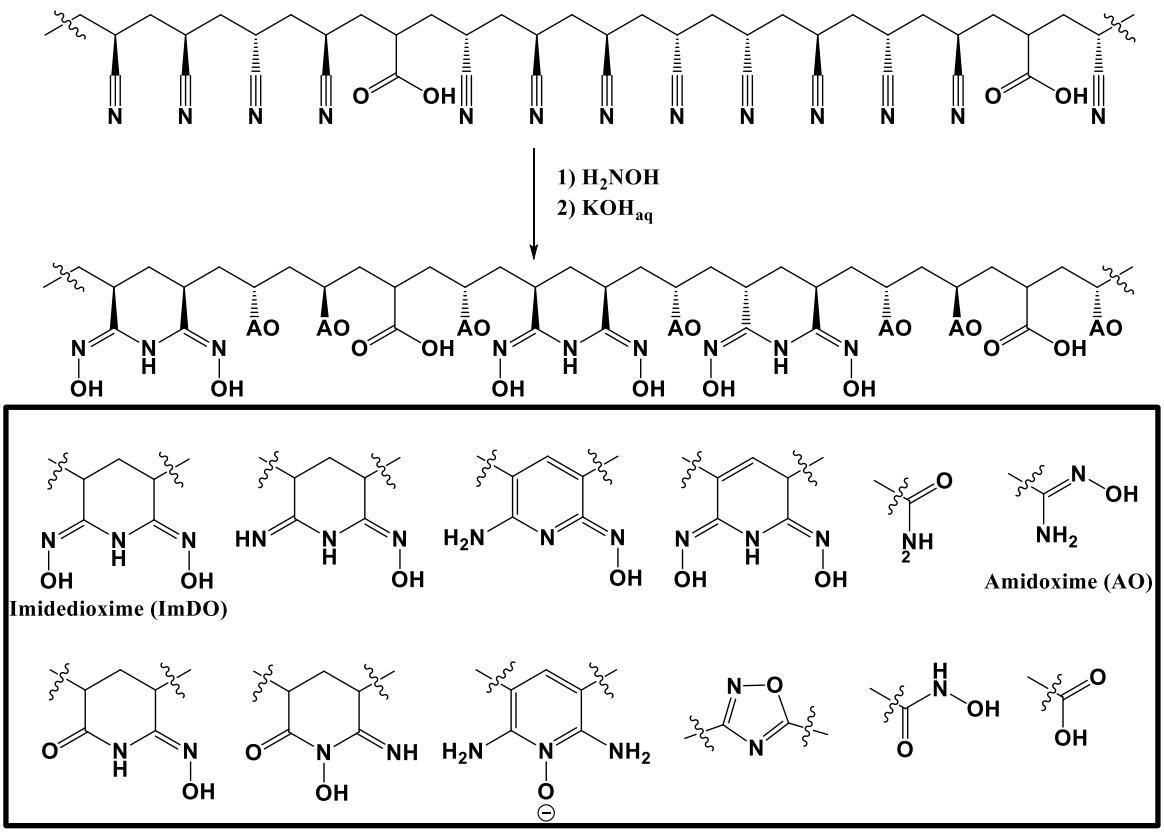

Figure 5: Functional groups that can be present on the fiber after hydroxylamine and base treatment.

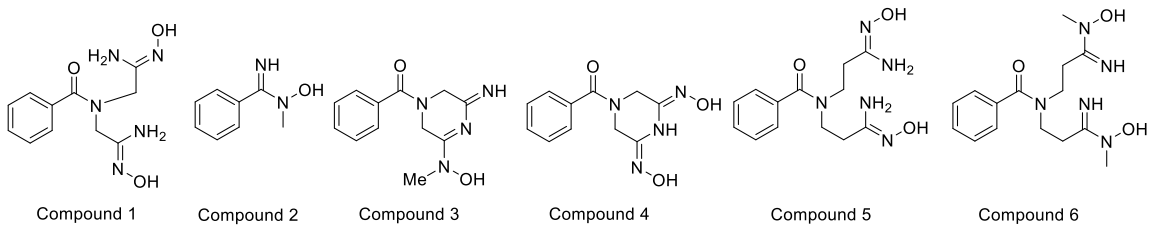

Figure 6: The binding constants of the above methylated amidoxime derivatives will be determined via complexometric titration. This will help us determine if the current method for predicting suitable small molecules for uranium extraction is viable or needs adjustments. This screening will provide a convenient way to predict bulk material performance, since the binding strength dictates the adsorbent selectivity. Compound 2 is named *N*-hydroxy-*N*-methylbenzimidamide, and Compound 3 is named (5-(hydroxy(methyl)amino)-3-imino-3,6-dihydropyrazin-1(2*H*)-yl)(phenyl)methanone.

Progress will be made towards the determination of whether small molecule analogues can be used as reliable proxies for complex polymers. It can be said with confidence that understanding of the physical model of both the small molecule and polymer fiber was enhanced through this research.

Method Background

Potentiometric Titration Methods

Titrations involve recording the cell potential (pH and millivolt (mv)) after each addition of titrant. Titrant is added in small amounts so that each recording is roughly 0.15 to 0.5 pH increments. After each addition of titrant enough time must be allowed for the solution to reach equilibrium before the recordings are taken, this is aided with nitrogen gas or magnetic stir bar. Nitrogen gas is not only used to aid mixing of the solution but also to purge the system of carbon dioxide from the atmosphere that could skew the potential measurements via the formation of carbonic acid.[41] Titrant is added starting from pH 2 and continuing until pH 12. Below pH 2 it is the hydronium ion and above pH 12 it is the hydroxide ion that are responsible for a large portion of the conductance, therefore glass electrode-reference electrode systems are only accurate between pH 2 and 12.[42]

Potentiometric Titration of free Ligand

Before performing a potentiometric titration, the number of dissociable protons can be predicted based on the ligand structure (Scheme 1). Using structural information, the chemical equilibria involved in the free ligand titration can also be predicted, shown in Table 1. These predictions will aid calculating the dissociation constants of the ligand.

The relationship between the stepwise protonation constants and the overall stability constants relates to the stability constants being the products of the cumulative protonation constants. For example: $\beta_{\mathrm{HL}} = K_1^{\mathrm{H}}$ and $\beta_{\mathrm{H_2L}} = K_1^{\mathrm{H}} \times K_2^{\mathrm{H}}$. In addition to the above equations there may also be concentrations of [OH^-] and [H^+] present in the solution. It is important to keep in mind that not all the above species will be present in any appreciable concentration throughout the entire pH range.

There are many ways to express protonation and complex formation equilibria in the literature. This section addresses the titration of the free ligand and the following example covers the equilibrium equations of the free ligand. Table 2 in the section on Potentiometric Titration of Ligand with Metal, uses Mg(II)-EDTA chelate as a more complex and thorough example of the terms most widely used.

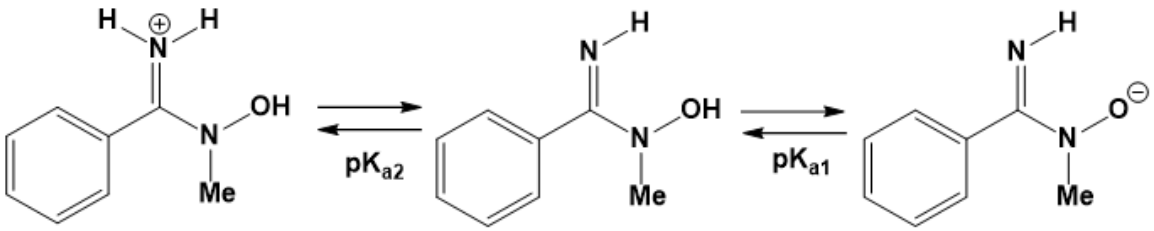

Scheme 1: Schematic representing the dissociation of *N*-hydroxy-*N*-methylbenzimidamide in aqueous solution.

Table 1: Stepwise and overall protonation equilibrium equations and constants for *N*-hydroxy-*N*-methylbenzimidamide.

Stepwise Protonation Equilibrium	Stepwise Protonation Constants	Overall Protonation Equilibrium	Overall Protonation Constants
$L^- + H^+ \leftrightharpoons HL$	$K_1^H = \frac{[HL]}{[L^-]\,[H^+]}$	$L^- + H^+ \leftrightharpoons HL$	$\beta_{HL} = \frac{[HL]}{[L^-]\,[H^+]}$
$HL + H^+ \leftrightharpoons H_2^+L$	$K_2^H = \frac{[H_2^+L]}{[HL]\,[H^+]}$	$L^- + 2H^+ \leftrightharpoons H_2^+L$	$\beta_{H_2L} = \frac{[H_2^+L]}{[L^-]\,[H^+]^2}$

Analysis of Potentiometric Titration of free ligand Data[43]

The equilibrium for a monoprotic acid LH when the number of moles equals 1 (n=1) that dissociates into its conjugate base L^- and H^+

$$\mathrm{LH} \underset{\leftrightharpoons}{\mathrm{K_a}} \mathrm{L^-} + \mathrm{H^+} \tag{1}$$

has the dissociation constant K_a.

$$\mathrm{K_a} = \frac{[\mathrm{H^+}][\mathrm{L^-}]}{[\mathrm{LH}]} = 10^{-\mathrm{pK_a}} \tag{2}$$

The average number of dissociable protons bound to the acid (ligand), $\overline{n}_{\mathrm{H}}$ is written mathematically as

$$\overline{n}_{\mathrm{H}} = \frac{\text{moles of bound } \mathrm{H^+}}{\text{total moles of weak acid}} = \frac{[\mathrm{LH}]}{[\mathrm{L^-}]+[\mathrm{LH}]} \tag{3}$$

Since the titrations occur in water the autoionization of water must also accounted for

$$\mathrm{H_2O} \underset{\leftrightharpoons}{K_\mathrm{w}} \mathrm{OH^-} + \mathrm{H^+} \tag{4}$$

Where the ion product K_w

$$K_\mathrm{w} = [\mathrm{OH^-}] + [\mathrm{H^+}] = 10^{-\mathrm{p}K_\mathrm{w}} \tag{5}$$

equals $10^{-13.787}$ at 0.1 M ionic strength at 25 °C. With

$$[\mathrm{H^+}] = 10^{-\mathrm{pH}} \tag{6}$$

and the concentration of hydroxide species being

$$[\mathrm{OH^-}] = \frac{K_\mathrm{w}}{[\mathrm{H^+}]} = 10^{-\mathrm{p}K_\mathrm{w}+\mathrm{pH}} \tag{7}$$

Keeping in mind the law of electroneutrality and that the concentration of all the anions and cations in solution must be equal

$$[\mathrm{L^-}] + [\mathrm{OH^-}] + [\mathrm{ClO_4^-}] = [\mathrm{Na^+}] + [\mathrm{H^+}] \quad (8)$$

$$[\mathrm{L^-}] = -[\mathrm{OH^-}] - [\mathrm{ClO_4^-}] + [\mathrm{Na^+}] + [\mathrm{H^+}] \quad (9)$$

Where the total concentration of the ligand is

$$\mathrm{L}_{tot} = [\mathrm{L^-}] + [\mathrm{LH}] \quad (10)$$

The average number of dissociable protons can then be represented as

$$\overline{n}_{\mathrm{H}} = \frac{\mathrm{L}_{tot} - [\mathrm{L^-}]}{\mathrm{L}_{tot}} \quad (11)$$

Substituting in eq 9,

$$\overline{n}_{\mathrm{H}} = \frac{\mathrm{L}_{tot} + [\mathrm{ClO_4^-}] - [\mathrm{Na^+}] - [\mathrm{H^+}] + [\mathrm{OH^-}]}{\mathrm{L}_{tot}} \quad (12)$$

For multiprotic species the moles of protons bound to the ligand is n times L_{tot}

$$\overline{n}_{\mathrm{H}} = \frac{n\mathrm{L}_{tot} + [\mathrm{ClO_4^-}] - [\mathrm{Na^+}] - [\mathrm{H^+}] + [\mathrm{OH^-}]}{\mathrm{L}_{tot}} \quad (13)$$

As the titrations proceed the concentrations of strong acid (*A*, from $HClO_4$) and weak acid (*L*, from the ligand) change. The total volume of the solution is changing throughout the titrations as well and needs to be considered (V_0 is the initial volume and *v* is the mL of added titrant, NaOH). The number of dissociable protons is represented by *n* and the average number of dissociable protons bound to the ligand is represented as, $\overline{n}_{\mathrm{H}}$.

$$\overline{n}_{\mathrm{H}} = n + \frac{\frac{A}{V_0+v} - \frac{C_b v}{V_0+v} - [\mathrm{H^+}] + [\mathrm{OH^-}]}{\frac{L}{V_0+v}} \quad (14)$$

This can also be expressed in terms of pH and pK_w

$$\overline{n}_{\mathrm{H}} = n + \frac{A - C_b v - (10^{-\mathrm{pH}} - 10^{-\mathrm{p}K_w + \mathrm{pH}})\,(V_0+v)}{L} \quad (15)$$

Using the data collected and the calculation performed above a difference plot (Bjerrum formation curve) can then be made of $\overline{n}_{\mathrm{H}}$ versus pH, which can help in the determination of the pK_a's of mono, di, and triprotic acids. From the difference plot the pK_a of a monoprotic acid is read at $\overline{n}_{\mathrm{H}} = 0.5$, for diprotic acids the pK_a's are read at $\overline{n}_{\mathrm{H}}$ =0.5 and 1.5, and for triprotic acids the pK_a's are read at $\overline{n}_{\mathrm{H}}$ =0.5, 1.5, and 2.5. A distribution graph of mole fraction vs corrected pH can also be made to visualize the mole fraction of each species present at each pH value.

The next step in the data analysis is curve fitting of the calculated, $\overline{n}_{\mathrm{H,calc}}$ value to the experimental value, $\overline{n}_{\mathrm{H,exp}}$ that was calculated above. The following equations are used to calculate $\overline{n}_{\mathrm{H,calc}}$

$$\mathrm{LH} \overset{\mathrm{K_a}}{\leftrightharpoons} \mathrm{L^-} + \mathrm{H^+} \tag{16}$$

$$\mathrm{K_a} = \frac{[\mathrm{H^+}][\mathrm{L^-}]}{[\mathrm{LH}]} = 10^{-\mathrm{pK_a}} \tag{17}$$

Using equation 3 and dividing by $[L^-]$ to get it in terms of pH and pK_a

$$\overline{n}_{\mathrm{H,calc}} = \frac{[\mathrm{LH}]}{[\mathrm{L^-}][\mathrm{LH}]} = \frac{\frac{[\mathrm{LH}]}{[\mathrm{L^-}]}}{\frac{[\mathrm{L^-}]}{[\mathrm{L^-}]} + \frac{[\mathrm{LH}]}{[\mathrm{L^-}]}} = \frac{\frac{[\mathrm{H^+}]}{[\mathrm{K_a}]}}{1 + \frac{[\mathrm{H^+}]}{[\mathrm{K_a}]}} \tag{18}$$

$$\overline{n}_{\mathrm{H,calc}} = \frac{\frac{10^{-\mathrm{pH}}}{10^{-\mathrm{pK_a}}}}{1 + \frac{10^{-\mathrm{pH}}}{10^{-\mathrm{pK_a}}}} = \frac{10^{\mathrm{pKa-pH}}}{1 + 10^{\mathrm{pKa-pH}}} \tag{19}$$

In this formalism $\overline{n}_{\mathrm{H,calc}}$ is independent of any concentration. In general, $\overline{n}_{\mathrm{H,calc}}$ is the weighted some of the mole fractions, α_j, of each protonated species (*j*) present in solution.

$$\overline{n}_{\mathrm{H,calc}} = \sum_{j=1}^{n} j\alpha_j \tag{20}$$

The mole fraction is calculated from

$$\alpha_j = \frac{\beta_j[\mathrm{H}^+]^j}{1 + \sum_{i=1}^{\mathrm{n}} \beta_i[\mathrm{H}^+]^i} \tag{21}$$

Where β is the protonation constant

$$\beta_j = \prod_{i=1}^{j} K_1 K_2 \ldots . K_j \tag{22}$$

The data is then fit in EXCEL using SOLVER, specifically the GRG Nonlinear solving method, which is used for smooth nonlinear data, to minimize mean absolute error (MAE) between the calculated (theoretical) and experimental (observed) $\overline{n}_{\mathrm{H}}$ values using equation 23. Keeping the experimentally determined value of $\overline{n}_{\mathrm{H,exp}}$ constant SOLVER varies the protonation constants β_j iteratively until the mean absolute error (S) in equation 23 is as small as mathematically possible. The data were weighted, and this is described later in this section in more detail.

$$S = \sum \left(\overline{n}_{\mathrm{H,exp}} - \overline{n}_{\mathrm{H,calc}}\right)^2 \tag{23}$$

The standard deviations (σ) for the pK_a's are then determined in EXCEL using the following equation

$$\sigma = \sqrt{\frac{1}{N}\sum_{i=1}^{N}(x_i - \mu)^2} \tag{24}$$

where μ is the mean, x_i is each individual value, and N is the number of values included in the data set.

Potentiometric Titration of Ligand with Metal

There are many ways to express protonation and complex formation equilibria in the literature. Table 2 uses Mg(II)-EDTA chelate as an example to not only cover the terms most widely used but also to illustrate the possible species that could be present and their corresponding stepwise and cumulative stability constants.

As a reminder, the relationship between the stepwise protonation constants and the cumulative stability constants is that the stability constants are the collective products of the protonation constants. In this case: $\beta_{\mathrm{HL}} = K_1^{\mathrm{H}}$, $\beta_{\mathrm{H_2L}} = K_1^{\mathrm{H}} \times K_2^{\mathrm{H}}$, $\beta_{\mathrm{H_3L}} = K_1^{\mathrm{H}} \times K_2^{\mathrm{H}} \times K_3^{\mathrm{H}}$, and $\beta_{\mathrm{H_4L}} = K_1^{\mathrm{H}} \times K_2^{\mathrm{H}} \times K_3^{\mathrm{H}} \times K_4^{\mathrm{H}}$. The magnesium (II) stepwise formation constant is identical to the overall constant: $\beta_{\mathrm{MgL}} = K_{\mathrm{MgL}}^{\mathrm{Mg}}$, whereas the cumulative formation constant is the product of the stepwise constants $K_{\mathrm{MgHL}}^{\mathrm{H}}$ and $K_{\mathrm{MgHL}}^{\mathrm{H}}$: $\beta_{\mathrm{MgHL}} = K_{\mathrm{MgHL}}^{\mathrm{H}} \times K_{\mathrm{MgL}}^{\mathrm{Mg}}$. In addition to the above equations there may also be concentrations of [OH^-], [H^+], as well as [Mg^{2+}] present in the solution. Not all the above species will be present in any appreciable concentration throughout the entire pH range.

Table 2. Stepwise and cumulative protonation equilibrium equations and constants for Mg(II)-EDTA chelate.

Stepwise Protonation Equilibrium	Stepwise Protonation Constants	Overall Protonation Equilibrium	Overall Protonation Constants
$L^{4-} + H^{+} \leftrightharpoons HL^{3-}$	$K_1^{H} = \frac{[HL^{3-}]}{[L^{4-}]\,[H^{+}]}$	$L^{4-} + H^{+} \leftrightharpoons HL^{3-}$	$\beta_{HL} = \frac{[HL^{3-}]}{[L^{4-}]\,[H^{+}]}$
$HL^{3-} + H^{+} \leftrightharpoons H_2L^{2-}$	$K_2^{H} = \frac{[H_2L^{2-}]}{[HL^{3-}]\,[H^{+}]}$	$L^{4-} + 2H^{+} \leftrightharpoons H_2L^{2-}$	$\beta_{H_2L} = \frac{[H_2L^{2-}]}{[L^{4-}]\,[H^{+}]^2}$
$H_2L^{2-} + H^{+} \leftrightharpoons H_3L^{-}$	$K_3^{H} = \frac{[H_3L^{-}]}{[H_2L^{2-}]\,[H^{+}]}$	$L^{4-} + 3H^{+} \leftrightharpoons H_3L^{-}$	$\beta_{H_3L} = \frac{[H_3L^{-}]}{[L^{4-}]\,[H^{+}]^3}$
$H_3L^{-} + H^{+} \leftrightharpoons H_4L$	$K_4^{H} = \frac{[H_4L]}{[H_3L^{-}]\,[H^{+}]}$	$L^{4-} + 4H^{+} \leftrightharpoons H_4L$	$\beta_{H_4L} = \frac{[H_4L]}{[L^{4-}]\,[H^{+}]^4}$
$Mg^{2+} + L^{4-} \leftrightharpoons MgL^{2-}$	$K_{MgL}^{Mg} = \frac{[MgL^{2-}]}{[L^{4-}]\,[Mg^{2+}]}$	$Mg^{2+} + L^{4-} \leftrightharpoons MgL^{2-}$	$\beta_{MgL} = \frac{[MgL^{2-}]}{[L^{4-}]\,[Mg^{2+}]}$
$MgL^{2-} + H^{+} \leftrightharpoons MgHL^{-}$	$K_{MgHL}^{H} = \frac{[MgHL^{-}]}{[MgL^{2-}]\,[H^{+}]}$	$Mg^{2+} + H^{+} + L^{4-} \leftrightharpoons MgHL^{-}$	$\beta_{MgHL} = \frac{[MgL^{2-}]}{[L^{4-}]\,[Mg^{2+}][H^{+}]}$
$Mg^{2+} + HL^{3-} \leftrightharpoons MgHL^{-}$	$K_{MgHL}^{H} = \frac{[MgHL^{-}]}{[Mg^{2+}]\,[HL^{3-}]}$		

Experiments Using Potentiometric Titration Method

The number of pH profiles needed depends on the molar ratio between the metal and ligand. When the approximate number of deprotonated sites on the ligand matches the coordination number of the metal in solution the molar ratio is effectively 1:1 as in the Mg(II)-EDTA chelate example shown above. Additional ratios should be designed to match the stoichiometry between the ligand and the metal ion. From these pH profiles stability constants can be calculated for the ligand metal complexes that are formed in the solution.

Calculation of Stability Constants from Potentiometric Titrations[43]

In potentiometric titrations $-\log[H^+]$ is the variable that is measured and is used in the computer program to calculate pH directly and minimize the sum of the weighted squares (described later) of the $-\log[H^+]$, this is done in a similar fashion as the Analysis of Potentiometric Titration of free ligand Data above. The algorithm used is shown below.[43]

$$\mathrm{T}_i = \sum_{j=1}^{\mathrm{NS}} e_{ij}\beta_j \prod_{k=1}^{i} [C_k]^{e_{ij}} \qquad (25)$$

Equation 25 is a" statement of the mass balance at a specific titration point of the *i*-th component in terms of the *j*-th species summed over all species present, NS. Each species concentration consists of a product of the overall stability constants and individual component concentrations $[C_k]$ raised to the power of the stoichiometric coefficient e*ij*."[43]

As an example, the Mg(II)-EDTA system consists of three components: $EDTA^{4-}$ (L), Mg^{2+} (M), and H^{+}. The species present are $HEDTA^{3-}$, H_2EDTA^{2-}, H_3EDTA^{-}, H_4EDTA, $MgEDTA^{2-}$, $MgHEDTA^{-}$, H^{+}, Mg^{2+}, and OH^{-}. There would then be three mass balance constraints: T_L for total ligand, T_M for total metal ion, and T_H for total initial hydrogen concentration.

$$T_L = [L^{4-}] + [HL^{3-}] + [H_2L^{2-}] + [H_3L^{-}] + [H_4L] + [MgL^{2-}] + [MgHL^{-}] \quad (26)$$

$$T_M = [Mg^{2+}] + [MgL^{2-}] + [MgHL^{-}] \quad (27)$$

$$T_H = [H^{+}] - [OH^{-}] + [HL^{3-}] + 2[H_2L^{2-}] + 3[H_3L^{-}] + 4[H_4L] + [MgHL^{-}] \quad (28)$$

As is implied by equation 25, the computer program that is used is set up in terms of β's, therefore the mass balance equations are rewritten in terms of their β values (stability constants) shown below in equations 29-31.

$$T_L = [L^{4-}] + \beta_{HL}[L^{4-}][H^{+}] + \beta_{H_2L}[L^{4-}][H^{+}]^2 + \beta_{H_3L}[L^{4-}][H^{+}]^3 + \beta_{H_4L}[L^{4-}][H^{+}]^4 + \beta_{MgL}[L^{4-}][Mg^{2+}] + \beta_{MgHL}[L^{4-}][Mg^{2+}][H^{+}] \quad (29)$$

$$T_M = [Mg^{2+}] + \beta_{MgL}[L^{4-}][Mg^{2+}] + \beta_{MgHL}[L^{4-}][Mg^{2+}][H^{+}] \quad (30)$$

$$T_H = \beta_{HL}[L^{4-}][H^{+}] + 2\beta_{H_2L}[L^{4-}][H^{+}]^2 + 3\beta_{H_3L}[L^{4-}][H^{+}]^3 + 4\beta_{H_4L}[L^{4-}][H^{+}]^4 + \beta_{MgHL}[L^{4-}][Mg^{2+}][H^{+}] + [H^{+}] - \beta_{OH}[H^{+}] \quad (31)$$

Each equation is simultaneously solved for each component $[C_k]$ (i.e. $[L^{4-}]$, $[Mg^{2+}]$, $[H^{+}]$) and then repeated for every equilibrium point taken. The value of $[H^{+}]$ calculated is then compared to the $[H^{+}]$ that was determined experimentally. The first calculations completed use both known and unknown β values, since there may be some previously known stability constants. Therefore 1) begin with known stability constants (β's) then calculate the hydrogen ion concentration at all points

then, 2) similarly to equation 21 calculate the weighted sum of the squares of the deviations in pH

$$S = \sum \mathrm{w}\left(\mathrm{pH}_{\mathrm{exp}} - \mathrm{pH}_{\mathrm{calc}}\right)^2 \quad (32)$$

where w is a weighing factor that lessens the influence of pH values that are not at accurate

$$\mathrm{w} = \frac{1}{(\mathrm{pH}_{i+1} - \mathrm{pH}_{i-1})^2} \quad (33)$$

after which, 3) you change the unknown β values and repeat the calculations until no further minimization is accomplished, which then provides the final stability constants.

Spectrophotometric Titrations[42]

When titrating strongly basic ligands it may not be possible to determine the protonation of the most basic form of the ligand, L^{n-}, before reaching pH 12. Since the accuracy of potentiometric titrations is limited to the pH range of 2-12. The protonation constants within the pH range of 2-12 are accurate; however, if the ligand does not fall within that range another method must be used.

Protonation and formation constants for the ligand and the associated metal complexes can be calculated using spectrophotometric titrations when the concentration of the free ligand, its acid forms, and metal ions are known. Keeping the ionic strength of the solution constant and using the hydroxide concentration to determine the stoichiometry of the solution, the pH range limitation of potentiometric titrations can be overcome.

Absorbance measurements can become complex when more than one species present absorbs at the same wavelength. This problem can be overcome by measuring the absorbance of the ligand and metal species separately before collecting absorbance of the metal-ligand complex. Spectrophotometric titrations measure absorbance according to the equation 34 below

$$\mathrm{A} = \log\frac{\mathrm{I_o}}{\mathrm{I}} = l\sum \epsilon_i \mathrm{C}_i \qquad (34)$$

where *l* is the path length of the cell, ϵ_i is the extinction coefficient of species *i*, C_i is the concentration of species *i*, I_o is the intensity of the incident light, and I is the intensity of the transmitted light. The values of the extinction coefficients of the metal ion and the ligand can be determined separately however, the extinction coefficients of all the complex species may not be easily determined from the data if their maximum concentrations were not obtained during the experimental run. Extinction coefficients as well as *β*'s can be determined if the experiments can be conducted over a range in which there is a sufficient change in the species concentration.

Spectrophotometric titrations can be used for measuring complex equilibria in aqueous solutions. The prediction of the free ligand, metal species, and metal-ligand species protonation and formation constants should be done in a similar fashion as discussed in section A.1.1. prior to collecting absorbance data. The hydrogen ion concentration must also be taken for each absorbance curve measurement. To determine the protonation and formation constants the combined data necessary.

Analysis of Spectrophotometric Data and Determination of β Values

The β values can be determined using equation 36 below which is derived from equation 34 above.

$$\mathrm{A} = l\left(\sum_{\mathrm{o}}^{\mathrm{n}} \epsilon_{\mathrm{n}}\,[\mathrm{ML_n}] + \sum \epsilon_{\mathrm{H}_{iL}}\,(\mathrm{H}_i\mathrm{L})\right)$$

$$= l\left(\epsilon_{\mathrm{M}}\,[\mathrm{M}] + \sum_{1}^{\mathrm{n}} \epsilon_{\mathrm{n}}\,\beta_{\mathrm{n}}[\mathrm{M}][\mathrm{L}]^{\mathrm{n}} + \sum \epsilon_{\mathrm{H}_i\mathrm{L}}\,[\mathrm{H}_i\mathrm{L}]\right) \qquad (35)$$

The known concentration values for each species are input along with all known β values. Theoretical absorbance data is calculated by finding the species half-equivalence point and the absorbance related to it. The data are then fit in Microsoft EXCEL using SOLVER, specifically the GRG Nonlinear solving method, which is used for smooth nonlinear data, which minimizes MAE by varying the β values in equation 34 and corresponding absorbance values in equation 36 below iteratively until the MAE error (S) in equation 36 is as small as it will get.

$$S = \sum\left(\mathrm{A}_{\mathrm{exp}} - \mathrm{A}_{\mathrm{calc}}\right)^2 \qquad (36)$$

CHAPTER THREE

MATERIALS AND METHODS

Materials

Materials used for the study of BIP and the first round of titrations of Compounds 1 and 2 are as follows: (> 98%) iron(III) nitrate nonahydrate (Lot #MKBL8206V), reagent grade (99% ACS) zinc heptahydrate (Batch #17215KB, reagent grade (< 99.0 %) iron(II) sulfate heptahydrate (Lot #119K1688), reagent grade (98%) nickel nitrate hexahydrate (Lot #001436016), zinc nitrate hexahydrate (Lot #MKBH2540V), and the reagent grade (99.9%) zinc sulfate monohydrate (Batch #04211MA) were purchased from Sigma Aldrich. The reagent grade (98%) copper(II) sulfate anhydrous (Lot #22056800) and the reagent grade (99.9%) nickel(II) chloride hexahydrate (Lot B5814020) were from Strem Chemicals. The buffer solutions were colorless NIST traceable solutions of pH 1.679, 4.005, 7.000, 10.012, and 12.45. The BIP molecule was suggested by Dr. Casey Johnson and prepared by Dr. Lyndsey Earl (ORNL postdocs) at ORNL. The pH meter used was a ThermoOrion model 420 with an Ag/AgCl electrode. The Varian Technologies Carey 5000 UV-Vis-NIR(Near-infrared) Spectrophotometer, Cary WinUV Scan program version 4.20.

Materials used for the most current titrations of Compounds #2 and #3 are as follows: The nickel(II) perchlorate hexahydrate (Lot #MKCCSS32), copper(II) perchlorate hexahydrate (Lot # MKB22944VS), iron(II) perchlorate hydrate, zinc

perchlorate hexahydrate (Lot #MKLD0198) were purchased from Sigma Aldrich. The reagent grade (62%) perchloric acid (Lot #16B033) was purchased from Alfa Aesar. The UO_2^{2+} source U 1000µg/mL in 2% HNO_3 (Lot #1326239) was purchased from High Purity Standards. The pH buffers used were Oakton, colorless, pH 1.68 (Lot #CC576185), pH 6.86 (Lot #CC546361), pH 9.18 (Lot #CC587154), pH 12.46 (Lot #CC579634), and Alfa Aesar, colorless, pH 4.01 (Lot # U21E020) purchased from Fischer Scientific. The methylated amidoxime derivatives, Compounds 1 and 2, were prepared by Dr. Ilja Popovs (ORNL) using typical secondary imine acylation procedures. The pH meter used was a VWR Symphony B10P (S/N 16072S0011), with a Thermo Scientific double junction pH Orion Ag/AgCl electrode probe (S/N 9102DJWP). The Ultraviolet-Visible spectrophotometer used was an Agilent Tech Carey Series UV-Vis, 1000 UV-Vis. Ultra-high purity nitrogen gas was used to purge the system and agitate the sample. A Polystat Cole Parmer temperature regulator was used to maintain a constant temperature.

BIP Methods

Solution Preparation

A stock solution of the BIP was prepared at 10^{-3} M in deionized water (Milli-Q, Waters Corp.) of >18MΩ·cm^{-1} resistivity using a 200 mL volumetric flask. Stock solutions of transition metals and uranium were prepared at 0.05 M in deionized water (Milli-Q, Waters Corp.) of >18MΩ·cm^{-1} resistivity from copper(II) nitrate

hexahydrate, iron(II) chloride anhydrous, nickel(II) chloride hydrate, uranyl nitrate hexahydrate, and zinc(II) nitrate hexahydrate. Stock solutions from 1 to 0.01 M of sodium hydroxide were prepared from purchased 10 M NaOH in 50 mL volumetric flasks. Stock solutions from 1 to 0.01 M of perchloric acid were prepared from purchased 62% $HClO_4$ in 50 mL volumetric flasks and stored in glass containers. Care was taken to store stock solution in the appropriate containers to prevent etching and degradation of the container and to prevent leeching into the solution.

Sample Preparation and Instrument Design

Ultraviolet-visible (UV-Vis) spectroscopy titrations for non-radioactive samples were performed using the Varian Technologies Carey 5000 UV-Vis-NIR(Near-infared) Spectrophotometer, Cary WinUV Scan program version 4.20 with 1.0 cm matched quartz cuvette cells at ORNL. Titrations containing uranium were carried out at the University of Tennessee in Buhler Hall. The scan method used was a double beam mode with zero/baseline correction, scanning the region from 450 nm to 190 nm. Reference solutions contained the same volume of deionized water at the same pH of the sample solution with the addition of base or acid to account for possible changes in the refractive index.[17] To ensure thorough mixing of the solution a magnetic star bar and plate was employed. The concentration of analyte used was low and careful attention was paid to precipitate formation during the titration experiment. When precipitation occurs (ligand precipitation, metal hydroxide formation[44]) the absorbance from the precipitate will overpower any absorbance from the analyte and will introduce error to the

absorbance measurements. Titrations of the BIP free ligand were run first to ensure that the peaks of interest fell between 0.1 and 1 absorbance units. A three neck flask was used to titrate 50 mL samples of 6 x 10^{-5} M BIP for all titrations; a similar titration method has been employed in previous publications.[16-18, 31] A ThermoOrion model 420 pH meter and a Ag/AgCl pH half-cell electrode with glass body were used and calibrated with NIST traceable buffer solutions of pH 1.679, 4.005, 7.000, 10.012, and 12.45 for all titrations.

The pH of the solution was initially adjusted to pH ~1.7 to allow for a titration that would span the largest range (~1.7 - ~13.5 pH units) as per previous methods.[17, 18, 31] Aliquots of sodium hydroxide (10 N to 0.01 N) were used to titrate the working and reference solutions in 0.15 to 0.5 pH unit increments. At every 0.15 to 0.5 pH unit increments a UV-Vis spectrum was collected, pH and potential (mV) were recorded. To maintain consistency complexometric titrations were run from start to finish in the same day without extended interruptions with an average experiment time of seven hours. A 1:1 ratio of BIP to metal was used during all BIP-Metal titrations. The metals investigated were uranium, zinc, copper, iron, and nickel.

Compounds #2 and #3 Methods

Solution preparation

Earlier titrations of Compounds #2 and #3 were done using the same solution preparation, sample preparation, and instrument design as the BIP

molecule, the latest titrations of Compounds 2 and 3 were done using the methods listed in this section.

Stock solutions of Compound #2 and #3 were prepared in varying concentrations using deionized water and 25 mL and 50 mL class A volumetric glassware. The concentrations of Compound 2 and 3 stock solutions were determined such that the smallest aliquot of stock solution was needed in order to render an absorbance peak of interest below 1 absorbance unit when analyzed in the UV-Vis, but still large enough to be measured and delivered using the auto pipettes. Stock solutions of Compound 1 and 2 needed to be made roughly every 6 months due to ligand degradation. Stock solutions of transition metals and uranium were prepared at 0.05 M in deionized water copper(II) nitrate hexahydrate, iron(II) chloride anhydrous, nickel(II) chloride hydrate, uranyl nitrate hexahydrate, and zinc(II) nitrate hexahydrate and in a later series of titrations from nickel(II) perchlorate hexahydrate, copper(II) perchlorate hexahydrate, iron(II) perchlorate hydrate, and zinc perchlorate hexahydrate. Stock solutions from 1.0 to 0.01 M of sodium hydroxide were prepared from purchased 10 N NaOH in 50 mL volumetric flasks. Stock solutions from 1.0 to 0.01 M of perchloric acid were prepared from purchased 62% $HClO_4$ in 50 mL volumetric flasks and stored in glass containers.

Sample Preparation and Instrument Design

Solutions of known concentrations were prepared by dilution from concentrated stock solutions. The desired ligand and metal concentrations for

each experiment were chosen so that when analyzed in the UV-Vis the absorbance peak of interest was between 0.1 and 1 Abs unit in a 1.0 cm pathlength cell. The samples were prepared by first adding DI water to a volumetric flask, adding the calculated volume of ligand, acid, and metal if needed. This sample solution was then added to a three-port European round bottom flask and all ports were sealed with parafilm or stopper. Each sample was analyzed the same day it was made.

The pH measurements were done using a VWR Symphony B10P (S/N 16072S0011), with a Thermo Scientific double junction pH Orion probe (S/N 9102DJWP) with an Ag/AgCl electrode. Prior to each pH measurement the pH probe and meter were calibrated using NIST colorless buffer solutions (1.68, 4.01, 6.86, 9.18, 12.46). The meters were standardized using 0.01 M $HClO_4$ and 0.01 M NaOH solutions and a calibration curve was fitted using the NERST slope and E° correction factors (Appendix Figure A-1).

UV-Vis spectroscopy was carried out on an Agilent Tech Carey Series UV-Vis, 1000 UV-Vis spectrophotometer, Cary WinUV program 4.20 with 1.0 cm match UV cells. A three-port jacketed flask was used as the titration vessel, it was connected to a constant temperature water bath that held the temperature constant at 25°C ±1°C.

The pH probe was inserted into the left flask port and the port opening was wrapped with parafilm to seal, a plug was inserted into the second port to seal, and the third port was used to sparge the solution with inert gas. The humidified

nitrogen was connected to a pasture pipette which was inserted into a hollowed rubber stopper. The second (middle) port was used to deliver aliquots of varying concentrations of sodium hydroxide throughout the experiment. After each addition of sodium hydroxide, a small sample of the solution was taken out of the flask and analyzed in the UV-Vis, after spectra were recorded it was returned to the flask and the titration continued until pH>12 or when the absorbance peak of interest was obstructed by the addition of sodium hydroxide.

The titrations were run following the same method outlined at the end of the Sample Preparation and Instrument Design section for the BIP Methods with the exception that the reference cell contained only DI water.

Data Analysis

The data were fit using Solver in Excel, to minimize mean absolute error (MAE) between the observed and theoretical absorbance data of at least two different wavelengths depending on the sample.[45] Theoretical absorbance data was calculated by finding the species half-equivalence point and the absorbance related to it. Solver minimizes MAE by varying the acid dissociation constant (pKa) values and corresponding absorbance values.[45] The Excel spreadsheet was designed and programed by Dr. Hancock at the University of North Carolina at Wilmington (UNCW). The selectivity and capacity of the ligand can be improved by examining the stability of the molecule through binding constants, or log(K) values,[18, 46, 47] as depicted below (Figure 7). Since the complexation constant is what conveys the binding strengths of the complex, and dissociation of a proton

from the ligand must occur before complexation, it is of critical importance to determine the acid dissociation constants.

$$HL \xrightarrow{K_a} L^- + H^+ \quad Dissociation \quad pK_a$$
$$L^- + M^{2+} \xrightarrow{K_1} ML^+ \quad Complexation \quad logK_1$$

Figure 7: Dissociation and complexation equations for pK_a and log(K).

CHAPTER FOUR

RESULTS AND DISCUSSION

BIP

An initial stock solution of BIP was prepared according to the methods listed previously however after six weeks it was observed that small crystals had formed in the BIP stock solution. As a change in ligand concentration directly influences interpretation of the data, a new solution was required. A 1.09×10^{-3} M BIP stock solution made previously by Dr. Lyndsay Earl was used as a substitute. The UV-Vis absorbance spectra of BIP made from stock #1 and #2 (Appendix Figures A-2 and A-3), it has been corrected to account for the change in volume throughout the titration. The wavelengths (nm) at which there was the most difference in absorbance between pH units were chosen to be analyzed in solver to determine pK_as (Appendix Table A-1). Corrected absorbance spectra of BIP free ligand (6×10^{-5} M) in aqueous solution from stock solution #1 (Appendix Figure A-4) which shows how closely the theoretical absorbance values are to the experimental values at varying pHs. Three acid dissociation constants were determined for the BIP free ligand over a pH range of 1.7 – 13.8 (Appendix Table A-2).

Referencing the structure of BIP below it is difficult to rationally link the dissociation constants determined for BIP with any of the expected protonation sites. Since the ligand precipitates out of solution below a pH of 5.0, pK_a values below 5.0 should not be able to be determined experimentally, however for both

cases they were determined as such by Solver (Figure 8, Appendix Figure A-5, Appendix Table A-2).

The pKa for a carboxylic acid is ~4.5. The BIP molecule has an extensively conjugated system with electron pair donors. It is thought that this will increase electron density of the carboxylic acids, raising the pH needed to deprotonate them. If this is true a pK_a below 5.0 is unlikely. In contrast, the pK_a for the conjugate acid of pyridine is ~5.25, while the conjugate acid of an imidazole is 7.05 and imidazole itself is > 12.7. The extensive conjugation poses the question whether discrimination between the deprotonation of each proton (i.e., the first carboxylic acid, the second carboxylic acid, the first imidazolium, the second imidazolium, then the pyridine) would be possible. The pK_a at 1.42 is not reliable, since precipitation occurs at a pH< 5.0 is due to protonation of the carboxylic acid sites, the pK_a at 5.04 is due to deprotonation of the conjugate acid of the pyridine, while the pK_a at 9.67 is due to the deprotonation of the conjugate acid of the imidazole.

The reduction in these values from their literature values suggests an overall electron withdrawing system which stabilizes a negative charge in solution, contradicting the electron donation within the ligand. This contradiction could be the result of experimental errors associated with measurement.

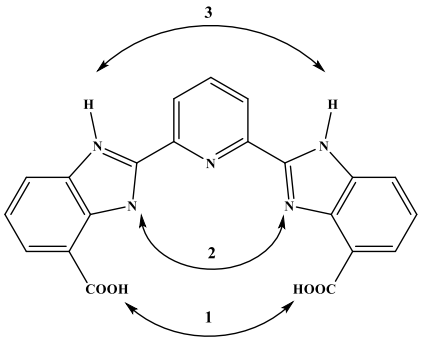

Figure 8: BIP showing three of the potentially five possible protonation's, there should be multiple isosbestic points.

Compound #2

The spectra for the titrations of Compound #2 and titrations of Compound #2 with the metals of interest (Appendix Figures A-6 through A-10, Appendix Tables A-3 through A-8) show clear isosbestic points which indicate a speciation change during the titration. Calculations yielded log(K) values for Cu^{2+} 11.06 ± 0.4, UO_2^{2+} 10.47 ± 0.5, Ni^{2+} 9.49 ± 0.01, Zn^{2+} 8.00 ± 0.05 which conveys a binding strength trend of $Cu^{2+} > UO_2^{2+} > Ni^{2+} > Zn^{2+}$.

After further titration training and consultation with Dr. Hancock it was decided that these types of titrations should be carried out with a reference solution of DI water only. If the reference solution contains a comparable solution to that of the sample, that being the reference sample is titrated along with the sample, there may be hydroxide formation or binding in the reference sample that is not occurring in the sample. After this decision was made all other titrations were performed using a reference solution that contained only water.

The spectra for the titrations of Compound #2 with a reference solution of DI water only (Appendix Figure A-11, A-12 and Tables A-9 through A-11). The pK_a values determined from the Zn^{2+} titration of 5.00 ± 0.05 and 8.26 ± 0.05 were similar the that in the solution when the reference solution was also titrated along with the sample, pK_as 4.89 ± 0.02 and 9.66 ± 0.04. The pK_a values determined from the Cu^{2+} titration of 4.39 ± 0.2 and 7.39 ± 0.4 were similar the that in the solution when the reference solution was also titrated, pK_as 4.91 ± 0.05 and 6.56 ± 0.3.

Compound #3

The spectra for the titrations of Compound #3 and titrations of Compound #3 with the metals of interest (Appendix Figures A-13 through A-15, Tables A-12, A-13) were carried out with a reference of DI water only and show a clear speciation change. Calculations yielded log(K) values for UO_2^{2+} 6.23 ± 0.2 and Zn^{2+} 7.43 ± 0.1 which conveys a binding strength trend of Zn^{2+}> UO_2^{2+}.

CHAPTER FIVE
RESEARCH CONCLUSIONS

Summary

The dissociation constants for BIP (Figure 3, page 7) free ligand with stock #2 support our earlier claim of an imidazole being net electron donating. This has an aspect of relativity – are the specific coordination of electron rich or electron poor relative to the rest of the molecule? Electron-pushing indicates the imidazole (literature pK_a >12.07) lone pair can push electron density onto the pyridine (literature pK_a ~5.25), making it electron rich. Similarly, it can push electron density onto the carboxylic acid (literature pK_a ~4.5), and vice-versa. So, all protonated sites are relatively electron rich, and therefore the values should shift to higher pK_a values compared to literature values, illustrated in Figure 9. Further investigation is needed before any definitive statements on exact electronic configurations can be made.

Based on previous research[16-18, 31] the pH was reduced from approximately 7 to below 2 using $HClO_4$ then titrated with increasing pH using sodium hydroxide to pH 13.5. This allowed for a titration that covered the entire reliable pH window, since water buffers below pH 2 and above pH 12 data collected in those regions are not accurate.[18] Achieving reliable spectra over this pH range turned out to be more challenging than initially anticipated. Due to BIP precipitating out of solution

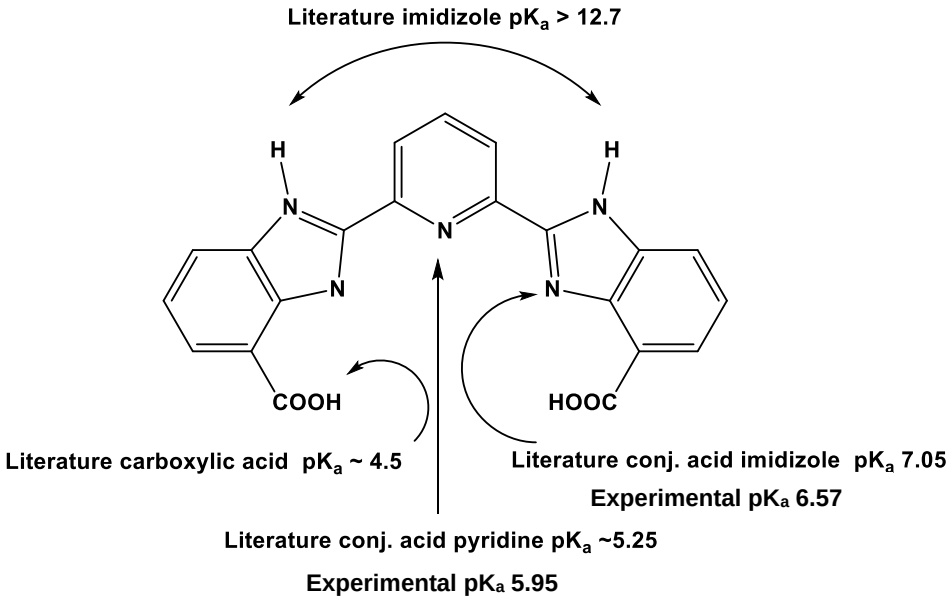

Figure 9: Electron pushing in BIP with literature and experimental pK_a values.

below pH 5.0, presumably due to protonation of the carboxylic acid functionalities and the concomitant decrease in overall molecular polarity.

This result was confirmed by a titration starting from the neutral pH and increasing acidity by pH increments of 0.1 to 0.5 using $HClO_4$. This suggests that all titrations in which the working solution was dropped below pH 5 prior to subsequent neutralization are not accurate.

Titrations of BIP with equal concentrations of metal were performed as well, with varying results. According to Hoffman Environmental Inc.,[44, 48] and their table on heavy metal ions and their respective solubility vs pH the metals should precipitate out as metal hydroxides as follows: Cu^{2+} pH 7, Ni^{2+} pH 9, and Zn^{2+} pH 8.2, and Iron(II)[49] should precipitate out as a hydroxide around pH 8. Nevertheless, in titrations of BIP and Cu, BIP and Zn, and BIP and Fe, BIP precipitated immediately upon addition of the metal. This was first thought to have been the BIP binding to the metal, however upon further investigation it was learned that BIP precipitates out kinetically below pH 5, this means that the precipitate does not readily dissolve in solution. Therefore, the precipitation seen during titrations in which BIP was run with metal was not the formation of metal hydroxide precipitates but the precipitation of the ligand in the acidic environment. BIP was rationally designed following promising computational experiments that offered several advantages including a binding pocket size that was tuned for larger ions, and a computationally determined stability constant in which uranyl bound stronger than the vanadium species (UO_2^{2+} log(K) 18.1, VO_2^{+} log(K) 7.4, and VO^{2+} log(K) 7.0).

However, experimentally it did turn out to have disadvantages which included low solubility and kinetic precipitation that inhibited the ability to confidently determine the pK_as and binding constants of this ligand.

Complexometric titrations were carried out on two of the methylated amidoxime derivates shown in Figure 6. The binding constants for Compound #2 with Cu (log(K) 11.06 ± 0.4), Ni (log(K) 9.49 ± 0.01), Zn (log(K) 8.00 ± 0.05), and U (log(K) 10.47 ± 0.5) were determined and the binding strength trend was Cu^{2+} > UO_2^{2+} > Ni^{2+} > Zn^{2+}, however these titrations were done with a reference cell that was titrated along with the sample, not DI water alone. When compared to the pK_a values of Compound #2 with Zn^{2+} and Cu^{2+} in which the reference cell contained only DI water there is a considerable difference in the dissociation constants and therefore the log(K) binding constants: the log(K) for Cu^{2+} was calculated to be 10.22 ± 0.5, and the log(K) for Zn^{2+} was calculated to be 9.40 ± 0.06. This difference may be due to the change in the method of treating the reference cell, titrating the cell or the cell containing only DI water. When using a comparable reference solution there may be unanticipated reactions occurring in the reference cell that are not occurring, or occurring at a different time, than in the sample cell. It was determined through this research that the method in which only DI water was used in the reference cell is a more accurate method of complexometric and spectrophotometric titrations.

The binding constants for Compound #3 with Zn^{2+}, and UO_2^{2+} were determined and the binding strength trend was Zn^{2+} > UO_2^{2+}, these titrations were

done with a reference cell that was DI water alone. When compared to the pK_a values of Compound #2 with Zn^{2+} and UO_2^{2+} there is a difference in the dissociation constants and therefore the log(K) binding constants: Compound #2 Zn^{2+} log(K) 9.40 ± 0.06 > Compound #3 Zn^{2+} log(K) 7.43 ± 0.1, and Compound #2 UO_2^{2+} log(K) 10.47 ± 0.5 > Compound #3 UO_2^{2+} log(K) 6.23 ± 0.2. These binding constants would indicate that Compound #2 binds more strongly to Zn^{2+} and UO_2^{2+} than Compound #3. Before this screening method can be determined to provide a convenient way to predict bulk material performance more complexometric titrations and research needs to be done on all compounds listed in Figure 6.

Future Directions

Complexometric and Spectrophotometric Titrations

While much was learned through this research further investigation of all compounds listed in Figure 6 needs to be completed before a more accurate picture can be made on the effectiveness of these small molecule analogs to adsorb uranyl and competing metals found in seawater. These studies would include titrations on all the small molecules listed with UO_2^{2+}, Ni^{2+}, Zn^{2+}, Cu^{2+}, Fe^{2+}, and vanadyl. Preliminary studies showed that ligand metal complexation titration with iron and vanadyl also had a kinetic component to them, so further kinetic studies on those metal complexations should also be done.

Coordination involved in Titrations

Potential Binding Modes

While titrations provide valuable information regarding the strength of uranyl binding, they provide very little insight regarding how uranyl is bound. Such information is essential for interpreting titration data, rationalizing adsorbent performance, and the development of new advanced materials. Nevertheless, there is no consensus regarding how amidoxime-functionalized polymers bind uranium during seawater recovery. Early small molecule crystal structures reported monodentate binding of acetamidoxime and benzamidoxime to the uranyl group through the oxime oxygen (Krebs group[50]), while simultaneous reports (Hay[30] and Rogers[29]) later reported amidoxime binds uranyl in an η^2 fashion (Figure 10a, and b). Theoretical insight from the Shi[51] group reported that coordination through the oxime oxygen atom and the amine nitrogen atom forming a five membered chelate ring (Figure 10c). The synthesis process of amidoxime-functionalized adsorbents is known to generate cyclic imide dioxime sites which have a particular affinity for uranyl as reported by Rao[21, 23, 52], and work by Warner[53] reported that cyclization of two adjacent amidoximes on glutardiamidoxime with uranium binding formed oxo-bridged dinuclear uranyl complexes (Figure 10d and e respectively).

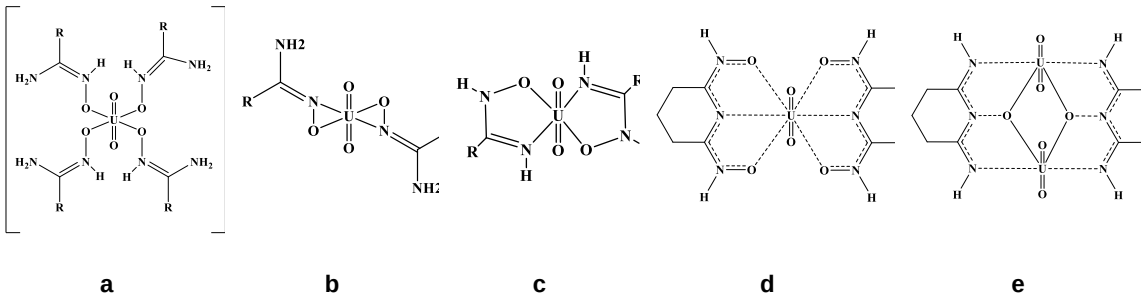

Figure 10: Chemical drawings of small molecule complexes to investigate how the ligands proposed binds uranyl. a) Monodentate binding of acetamidoxime to the uranyl group through the oxime oxygen, b) η^2 binding mode, amidoxime binding to uranyl with the nirtorgen and oxygen of the oxime group, c) κ^2 binding mode, coordination through the oxime oxygen and the amine nitrogen atoms forming a five membered chelate ring, d) cyclic imide dioxime, e) oxo-bridged dinuclear uranyl complex.

Computationally-guided design of a uranyl chelator was reported by Vukovic[28] and his team that proposed a method for computationally predicting chelators that would have strong bonding and selectivity towards uranium, assuming an η^2 binding mode is achieved, as predicted for binding of uranyl by non-cyclic amidoxime small molecules. [29, 51] Computationally predicted pre-organized uranyl receptors were titrated by Mehio[17, 18, 31] and Lashley[16] and showed promise in terms of bond strength, however, they did not perform well when grafted onto a polymer support. An emerging trend is that rationally-designed small molecule uranyl receptors do not perform as expected when grafted onto fibers.

There are noteworthy differences between the small molecule and polymers pK_as determined through complexometric titrations and potentiometric titrations, respectively. These differences in pK_as are indicative of different binding strength, and potentially different biding modes between the small molecules and the polymers. The extent to which the binding strengths vary between the small molecule analogues and the polymers should be investigated further.

Work done by Abney[34, 35] *et al* indicates small molecule analogues possess different extended x-ray absorption fine structure (EXAFS) spectra than adsorbents contacted with uranium in a brine solution, while seawater-contacted adsorbents possess an even more divergent spectra, suggestive of an adjacent transition metal in the uranium binding environment. Two theories could explain this observed discrepancy, with the first being that amidoximation by-products are

doing the binding. This is supported by the observation that < 1% of all U-binding sites are occupied upon adsorbent saturation, numerous reaction by-products are theoretically possible, and that little work has been done to characterize the polymer itself, after amidoximation and KOH conditioning. The second theory is that the morphology of the adsorbent influences the uranium binding mode, which is supported by the alleged transition metal adjacent to the uranium from the EXAFS work and that distinctly different spectra were obtained for adsorbent samples contacted in seawater and brine.[34, 35]

To resolve this controversy, amidoxime derivative small molecules have been designed to act as proxies for several potential uranium-binding sites in polymeric adsorbents (Figure 11). Methylated amidoximes, with the methyl-group on the oxime nitrogen (Figure 11, Compounds 2, 3, and 6) are expected to force the κ^2 (chelating) coordination motif as is proposed from EXAFS studies.[34, 35] The oxime-methyl group will disrupt the structure such that the η^2-coordination motif observed in single crystal studies is not possible since the nitrogen atom would exceed an allowable valency (Figure 2). If this hypothesis proves to be true the EXAFS studies of Compounds 1, 4, and 5 will show the η^2-coordination motif while the others show κ^2 (chelating) coordination motif. During polymerization cyclization can occur between adjacent functional groups which produces a polymer that has cyclized positions and non-cyclized moieties. In a continued effort to probe the polymer Compounds 3 and 4 were chosen to represent cyclized binding sites while

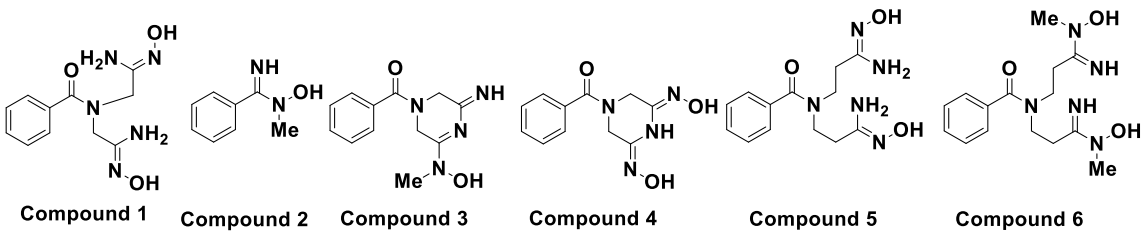

Figure 11: Methylated and on methylated amidoxime derivative compounds proposed.

due to the addition of carbon on the chain Compounds 5 and 6 represent the non-cyclic potential binding sites.

Investigation of Potential Binding Modes

Previous investigations[18] into amidoximes and amidoximated polymers for uranyl adsorbent studies focused solely on the amidoxime functional group and investigating its protonation and formation constants. Through those studies it has been found that less than 1% of the functional groups on the polymer bind uranyl and it is still not understood which specific functional groups on the polymer are binding uranyl. By investigating the rest of the polymer and some of the other functional groups that are created through the polymerization process including byproducts progress can be made towards determining the specific groups on the polymer that are binding to uranyl.

From spectrophotometric titrations the number of dissociable protons, pK_a's, and formation constants of various ligands with metal cations can be determined. This information can be used to help guide ligand design and maximize sites that improve uranyl uptake. However, further investigation using X-ray adsorption fine structure (XAFS) spectroscopy and X-ray crystallography will be needed to determine the specific binding modes of the ligands more definitively with uranyl.

In conjunction with spectrophotometric titrations, crystals of the ligands bound to uranyl will also be investigated through X-ray crystallography. X-ray crystallography gives information regarding the lattice structure, including bond

length, bond angles, cell dimensions, and site ordering details. From X-ray crystallography, single crystal refinement will also be performed to obtain the crystal structure and therefore the coordination environment and binding mode of these small molecule systems. Several methods of growing crystals will be employed, including slow evaporation, slow cooling, vapor diffusion, and liquid-liquid diffusion. While X-ray crystallography is a powerful method in determining binding modes it must be noted that the information gained is for small molecule crystals only and may not accurately represent the binding mode or modes present on the polymer in aqueous solution, and therefore must be used in conjunction with other spectroscopy techniques.

To identify the uranyl coordination environment of contacted polymers XAFS spectroscopy will need to be used to investigate the amidoxime-functionalized polymers exposed to seawater and seawater simulant. This technique has been used with success by Abney et al.[34, 35] We will look at both solid phase systems, as well as wetted solid polymers in an aqueous matrix. By fitting in the extended XAFS (EXAFS) region the local atomic structure of uranyl and its coordination can be investigated. The data gained from EXAFS more accurately reflects the polymer environment than the single crystal X-ray studies.

By investigating this series of methylated amidoxime derivatives further and the associated polymers, we could rationally test the EXAFS-proposed binding mode, while obtaining binding constants of Compounds 1, 4-6 (Figure 6).

LIST OF REFERENCES

1. Nuclear Energy Agency., Uranium 2009: Resources, Production and Demand. Paris, 2010.
2. Beverly, R. G.; Cleveland, J. E.; Hughes, P. R., Impacts of Uranium Mining on the Environment. 1983.
3. Davies, R. V.; Kennedy, J.; McIlroy, R. W.; Spence, R.; Hill, K. M., Extraction of Uranium from Sea Water. *Nature* **1964,** *203*, 1110-1115.
4. Seko, N.; Katakai, A.; Hasegawa, S.; Tamada, M.; Kasai, N.; Takeda, H.; SUgo, T.; Saito, K., Aquaculture of Uranium in Seawater by a Fabric Adsorbent Submerged System. *Nucl. Technol.* **2003,** *144*, 274.
5. Tamada, M., Technolgy of uranium recovery from seawater. *Jpn. Inst. Energy* **2009,** *88*, 249-253.
6. Endrizzin, F.; Leggett, C. J.; Rao, L., Scientific Basis for Efficient Extraction of Uranium from Seawater: Understanding the Chemical Speciation of Uranium under Seawater Conditions. *Ind. Eng. Chem. Res.* **2016,** *55*, 4249-4256.
7. Choppin, G. R., Soluble Rare Earth adn ACtinide Species in Seawater. *Mar. Chem.* **1989,** *28*, 19-26.
8. Suzuki, T.; Saito, K.; Sugo, T.; Ogura, H.; Oguma, K., Fractional elution and determination of uranium and vanadium adsorbed on amidoxime fiber from seawater. *Anal. Sci.* **2000,** *16* (4), 429-432.
9. Wang, L.; Meng, C.; Ma, W., Preparation of lithium ion-sieve and utilizing recoveryof lithium from seawater. *Front. Chem. Eng. China* **2009,** *3*, 65-67.
10. Tamada, M. In *Current status of technology for collection of uranium from seawater*, Erice Seminar, Japan Atomic Energy Agency, Japan, Japan, 2009; pp 1-9.
11. Astheimer, L.; Schenk, H. J.; Witte, E. G.; Schwochau, K., Development of Sorbers for the Recovery of Uranium from Seawater. Part 2. The Accumulation of Uranium from Seawater by Resins Containing Amidoxime and Imidoxime Functional Groups. *Sep. Sci. Technol.* **1983,** *18* (4), 307-339.
12. Schenk, H. J.; Astheimer, L.; Witte, E. G.; Schwochau, K., Development of Sorbers for the Recovery of Uranium from Seawater. 1. Assessment of Key Parameters and Screening Studies of Sorber Materials. *Sep. Sci. Technol.* **1982,** *17* (11), 1293-1308.
13. Kim, J.; Tsouris, C.; Mayes, R. T.; Oyola, Y.; Saito, T.; Janke, C. J.; Dai, S.; Schneider, E.; Sachde, D., Recovery of Uranium from Seawater: A Review of Current Status and Future Research Needs. *Sep. Sci. Technol.* **2013,** *48* (3), 367-387.
14. Lindner, H.; Schneider, E., Review of cost estimates for uranium recovery from seawatrer. *Energy Econ.* **2015,** *49*, 9-22.
15. Kim, J.; Tsouris, C.; Oyola, Y.; Janke, C. J.; Mayes, R. T.; Dai, S.; Gill, G.; Kuo, L.-J.; Wood, J.; Choe, K.-Y.; Schneider, E.; Lindner, H., Uptake of Uranium from Seawater by Amidoxime-Based Polymeric Adsorbent: Field Experiments, Modeling, and Updated Economic Assessment. *Ind. Eng. Chem. Res.* **2014,** *53*, 6076-6083.

16. Lashley, M. A.; Ivanov, A. S.; Bryantsev, V. S.; Dai, S.; Hancock, R. D., Highly Preorganized Ligand 1,10-Phenanthroline-2,9-dicarboxylic Acid for the Selective Recovery of Uranium from Seawater in the Presence of Competing Vanadium Species. *Inor. Chem.* **2016,** *55* (20), 10818-10829.
17. Mehio, N.; Ivanov, A. S.; Williams, N. J.; Mayes, R. T.; Bryantsev, V. S.; Hancock, R. D.; Dai, S., Quantifying the binding strength of salicylaldoxime-uranyl complexes relative to competing salicylaldoxime-transition metal ion complexes in aqueous solution: a combined experimental and computational study. *Dalton. Trans.* **2016,** *45* (22), 9051-9064.
18. Mehio, N.; Lashley, M. A.; Nugent, J. W.; Tucker, L.; Correia, B.; Do-Thanh, C.; Dai, S.; Hancock, R. D.; Bryantsev, V. S., Acidity of the Amidoxime Functional Group in Aqueous Solution: A Combined Experimental and Computational Study. *J. Phys. Chem. B* **2015,** *119*, 3567-3576.
19. Tomomi, K.; Saito, K.; Kazuyuki, S.; Takshi, K.; Kanno, J.;, Katakai, A.; Seko, N.; Sugo, T., Preparation of hydrophilic amidozime fibers bcografting acrylonitrile and methacrylic acid from an optimized monomer composition. *Rad. Phys. And. Chem.* **2000,** *59*, 405-411.
20. ORNL, Photo courtesy of Oak Ridge National Laboratory. 2016.
21. Tian, G.; Teat, S.; Rao, L., Thermodynamic studies of U(VI) complexation with glutardiamidoxime for sequestration of uranium from seawater. *Dalton. Trans.* **2013,** *42* (16), 5690-5696.
22. Sun, X.; Xu, C.; Tian, G.; Rao, L., Complexation of glutarimidedioxime with Fe(iii), Cu(ii), Pb(ii), and Ni(ii), the competing ions for the sequestration of U(vi) from seawater. *Dalton. Trans.* **2013,** *42* (40), 14621-14627.
23. Tian, G.; Teat, S.; Zhang, Z.; Rao, L., Sequestering uranium from seawater: binding strength and modes of uranyl complexes with glutarimidedioxime. *Dalton. Trans.* **2012,** *41* (38), 11579-11589.
24. Leggett, C. J.; Parker, B. F.; Teat, S. J.; Zhang, Z.; Dau, P. D.; Lukens, W. W.; Peterson, S. M.; Cardenas, A. J. P.; Warner, M. G.; Gibson, J. K.; Arnold, J.; Rao, L., Structural and spectroscopic studies of a rare non-oxido V(v) complex crystallized from aqueous solution. *Chem. Sci.* **2016,** *7* (4), 2775-2786.
25. Kang, S. O.; Vukovic, S.; Custelcean, R.; Hay, B. P., Cyclic Imide Dioximes: Formation and Hydrolytic Stability. *Ind. Eng. Chem. Res.* **2012,** *51* (19), 6619-6624.
26. Grant, C. D.; Kang, S. O.; Hay, B. P., Synthesis of a Hydrophilic Naphthalimidedioxime. *J. Org. Chem.* **2013,** *78* (15), 7735-7740.
27. Chatterjee, S.; Bryantsev, V. S.; Brown, S.; Johnson, J. C.; Grant, C. D.; Mayes, R. T.; Hay, B. P.; Dai, S.; Saito, T., Synthesis of Naphthalimidedioxime Ligand-Containing Fibers for Uranium Adsorption from Seawater. *Ind. Eng. Chem. Res.* **2015,** *55* (15), 4161-4169.
28. Vukovic, S.; Hay, B. P., De Novo Structure-Based Design of Bis-amidoxime Uranophiles. *Inor. Chem.* **2013,** *52* (13), 7805-7810.

29. Barber, P. S.; Lelley., S. P.; Rogers, R. D., Highly selective extraction of the uranyl ion with hydrophobic amidoxime-functionalized ionic liquids via n2 coordination. *RSC Adv* **2012,** *2*, 8526-8530.
30. Vukovic, S.; Watson, L. A.; Kang, S. O.; Custelcean, R.; Hay, B. P., How Amidoximate Binds the Uranyl Cation. *Inor. Chem.* **2012,** *51* (6), 3855-3859.
31. Mehio, N.; Williamson, B.; Oyola, Y.; Mayes, R. T.; Janke, C.; Brown, S.; Dai, S., Acidity of the Poly(acrylamidoxime) Adsorbent in Aqueous Solution: Determination of the Proton Affinity Distribution via Potentiometric Titrations. *Ind. Eng. Chem. Res.* **2016,** *55* (15), 4217-4223.
32. McKenzie, B. M.; Miller, A. K.; Wojtetcki, R. J.; Johnson, J. C.; Burke, K. A.; Tzeng, A. K.; Mather, P. T.; Rowan, S. J., Improved synthesis of functionalized mesogenic 2,6-bisbenzimidazolypyridine ligands. *Tetrahedron* **2008,** *64* (36), 8488-8495.
33. Wojtetcki, R. J.; Wu, Q.; Johnson, J. C.; Ray, D. G.; Korley, L. T. J.; Rowan, S. J., Optimizing the formation of 2,6-bis(N-alkyl-benzimidazolyl)pyridine-containing [3]catenates through component design. *Chem. Sci.* **2013,** *4* (12), 4440-4448.
34. Abney, C. W.; Das, S.; Mayes, R. T.; Kuo, L.-J.; Wood, J.; Gill, G.; Piechowicz, M.; Lin, Z.; Lin, W.; Dai, S., A Report of Emergent Uranyl Binding Phenomena by an Amidoxime Phosphonic Acid Co-Polymer. *Phys. Chem. Chem. Phys.* **2016,** *18 (34)*, 23462-23468.
35. Abney, C. W.; Mayes, R. T.; Piechowicz, M.; Lin, Z.; Bryantsev, V.; Veith, G. M.; Dai, S.; Lin, W., XAFS Investigation of Polyamidoxime-Bound Uranyl Contests the Paradigm from Small Molecule Studies. *Energy Environ. Sci.* **2016,** *9* (2), 448-453.
36. Pan, H.; Lao, W.; Wai, C. M.; Oyola, Y.; Janke, C. J.; Tian, G., Rao, L., Carbonate-H_2O leaching sequestering uranium from seawater. *Dalton. Trans.* **2014,** *43*, 10713-10718.
37. Das, S.; Lio, W.-P.,; Bryers, M. F.; Tsouris, C.; Janke, C. J.; Mayes, R. T.: Schneider, E.; Kuo, L.-J.; Wood, J. R.; Gill, G. A.' Dai, S., Alternative Alkaline Conditioning of Amidoxime Based Adsorbent for Uranium Extraction from Seawater. *Ind. Eng. Chem. Res.* **2016,** *55* (15), 4303-4312.
38. Das, S.; Oyola, Y.; Mayes, R. T.; Janke, C. J.; Kuo, L.-K.; Gill, G.; Wood, J. R.; Dai, S., Extracting Uranium from Seawater: Promising AF Series Adsorbents. *Ind. Eng. Chem. Res.* **2016,** *55* (15), 4110-4117.
39. Barot, N. R.; Elvidge, J. A., Heterocyclic imines and amines. Part XII. Imino-derivatives of piperazine. *J. Chem. Soc.* **1972,** *Perkin Trans I*, 1009-1014.
40. Barot, N. R.; Elvidge, J. A., Heterocyclic imines and amines. Part XVI. 2,6-Diaminopyrazine and its 1-oxide from iminodiacetonitrile. *J. Chem. Soc.* **1973,** *Perkins Trans. 1*, 606-612.
41. McAlpine, R. K., The carbon dioxide problem in neutralization titrations. *J. Chem. Ed.* **1944,** *21* (12), 589.
42. Martell, A. E.; Hancock, R. D., *Metal Complexes in Aqueous Solutions*. 1st ed.; Springer Schience: New York, 1996.

43. Martell, A. E.; Motekaitis, R. J., *Determination and Use of Stability Constants*. 2nd ed.; VCHS Publishers: New York, 1992.
44. Hoffland Environmental, Inc. Hydroxide Precipitation of Metals. https://heienv.com/hydroxide-precipitation-of-metals/.
45. Billo, E. J., *EXCEL for Chemists*. 3rd ed.; Wiley- CH: Wiley- CH, 2011.
46. Barnum, D., Predicting Acid-Base Titration Curves without calculations. *J. Chem. Ed.* **1999,** *76* (7), 938-942.
47. Kraft, A., The determination of the pKa of Multiprotic, Weak Acids by Analyzing Potentiometric Acid-Base Titration Data with Different Plots. *J. Chem. Ed.* **2003,** *80* (5), 554-559.
48. Albrecht, T. W. J.; Addai-Mensah, J.; Fornasiero, D., *Effect of pH, Concentration and Temperature on Copper and Zinc Hydroxide Formation/Precipitation in Solution*.
49. Morgan, B.; Lahav, O., The effect of pH on the kinetics of spontaneous Fe(II) oxidation by O2 in aqueous solution - basic principles and a simple heuristic description. *CHemosphere* **2006,** *68* (2007), 2080-2084.
50. Witte, E. G.; Schwochau, K. S.; Henkel, G.; Krebs, B., Uranyl complexes of acetamidoxime and benzamidoxime Preparation, characterization, and crystal structure. *Inorg. Chim. Acta.* **1984,** *94*, 323-331.
51. Wang, C.; Lan, J.; Wu, Q.; Luo, Q.; Zhao, Y.; Wang, X.; Chai, Z.; Shi, W., Theoretical Insights on the Interaction of Uranium with Amidoxime and Carboxyl Groups. *Inor. Chem.* **2014,** *53*, 9466-9476.
52. Endrizzi, F.; Melchior, A.; Tolzzi, M.; Rao, L., Complexation of uranium (VI) with glutarimidoxioxime: thermodynamic and computational studies. *Dalton. Trans.* **2015,** *44*, 13835-13844.
53. Kennedy, Z. C.; Cardenas, A. P.; Corbey, J. F.; Warner, M. G., 2, 6-Diiminopiperidin-1-ol: an overlooked motif relevant to uranyl transition metal binding on poly(amidoxime)adsorbents. *Chem. Comm.* **2016,** *52*, 8802-8805.

APPENDIX

NERST Data

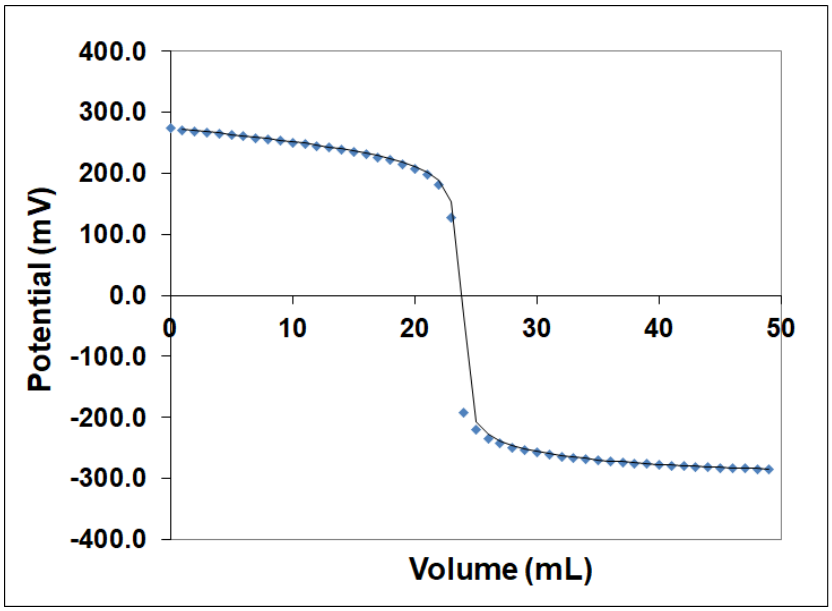

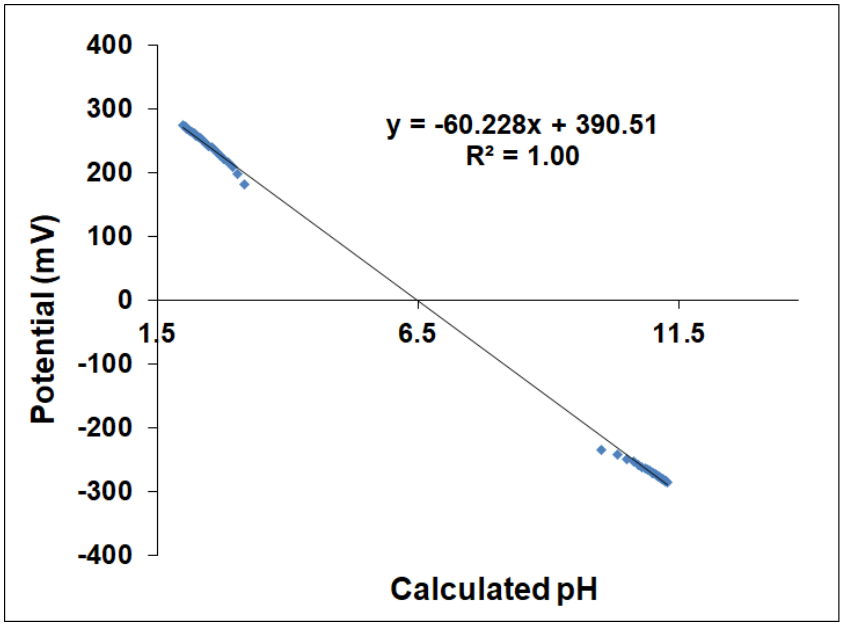

Figure A-1: (Top) Strong acid (0.01 M HClO4) versus strong base (0.01 M NaOH) titration used to standardize the pH electrode. The initial solution contained 25 mL of 0.01 M HClO4. (Bottom) Calibration plot used to determine the Nernst slope (-60.228) and the E^o correction factor (390.51).

BIP Data and Results

Table A-1: Dissociation constant comparison between BIP Stock #1 and #2.

BIP Free Ligand Stock #1, prepared by KM			BIP Free Ligand Stock #2, prepared by LE		
Dissociation Constants	Wavelength (nm)	Std Dev	Dissociation Constants	Wavelength (nm)	Std Dev
1.42, 5.95, 6.57	283	0.0035	1.33, 8.21, 8.86	283	0.0020
	313	0.0037		345	0.0012
	347	0.0035		366	0.0047

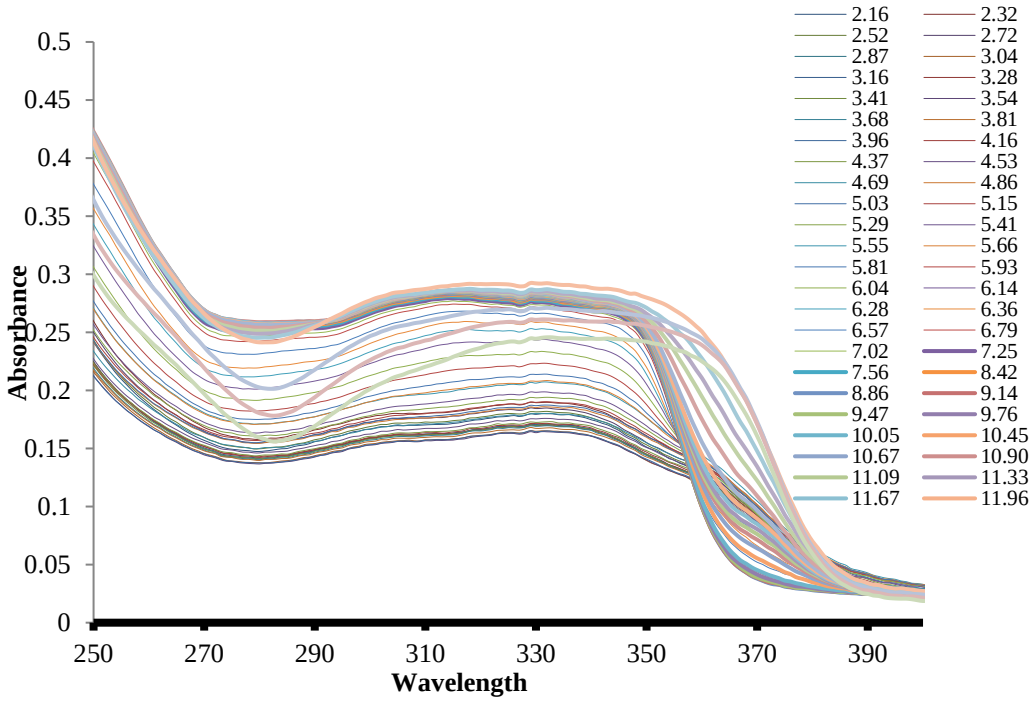

Figure A-2: Spectra of benzamidizolepyrodine (BIP) ($6x10^{-5}$ M) in aqueous solution using the stock solution #1, previously prepare by K.C. Mote. The corresponding pH values are listed to the right of the spectra.

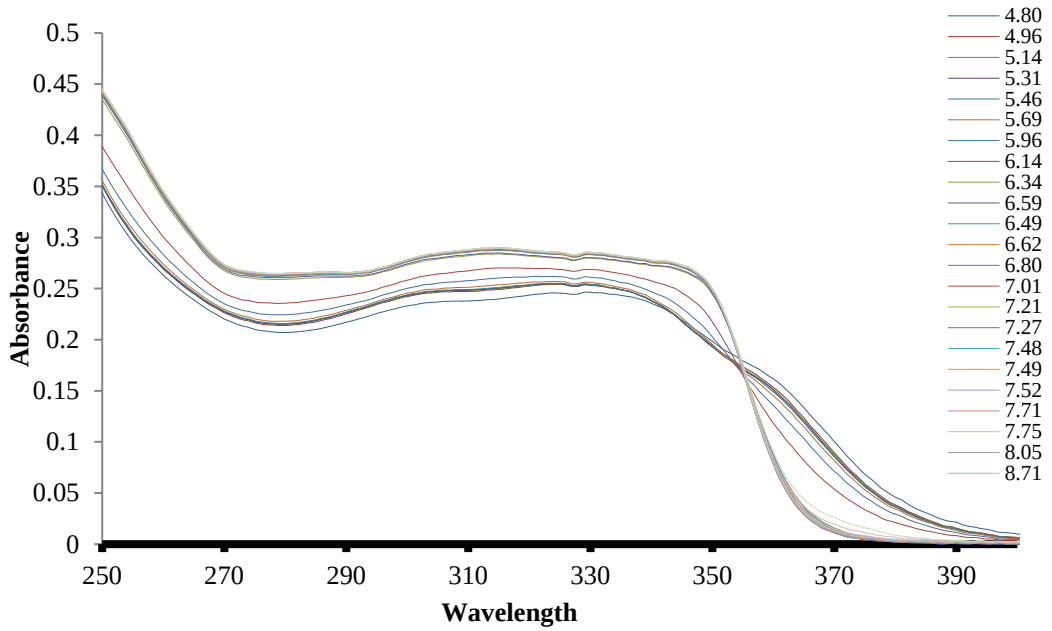

Figure A-3: Spectra of benzamidizolepyrodine (BIP) ($6x10^{-5}$ M) in aqueous solution using the stock solution #2, previously prepare by Dr. Lyndsey Earl.

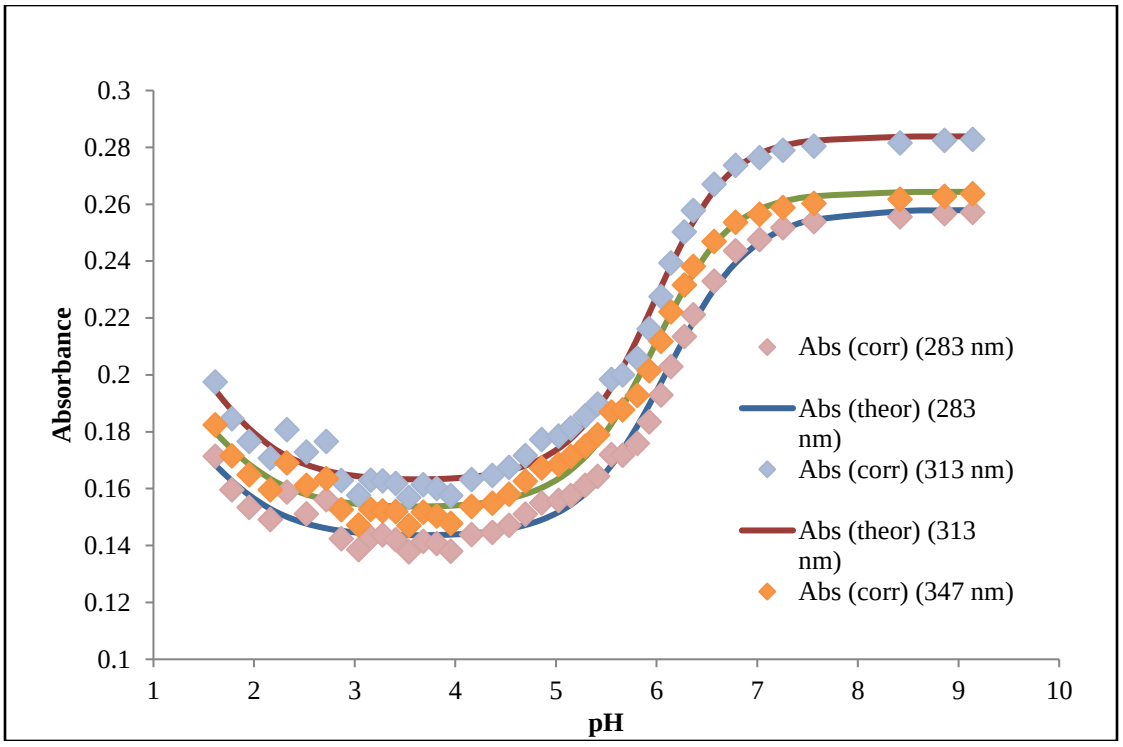

Figure A-4: Variation of absorbance at three different wavelengths of $6x10^{-5}$ M benzamidizolepyrodine (BIP) ($6x10^{-5}$ M) in aqueous solution using the stock solution #1. The points are experimental values, and the solid lines are theoretical curves fitted to the data using Solver.

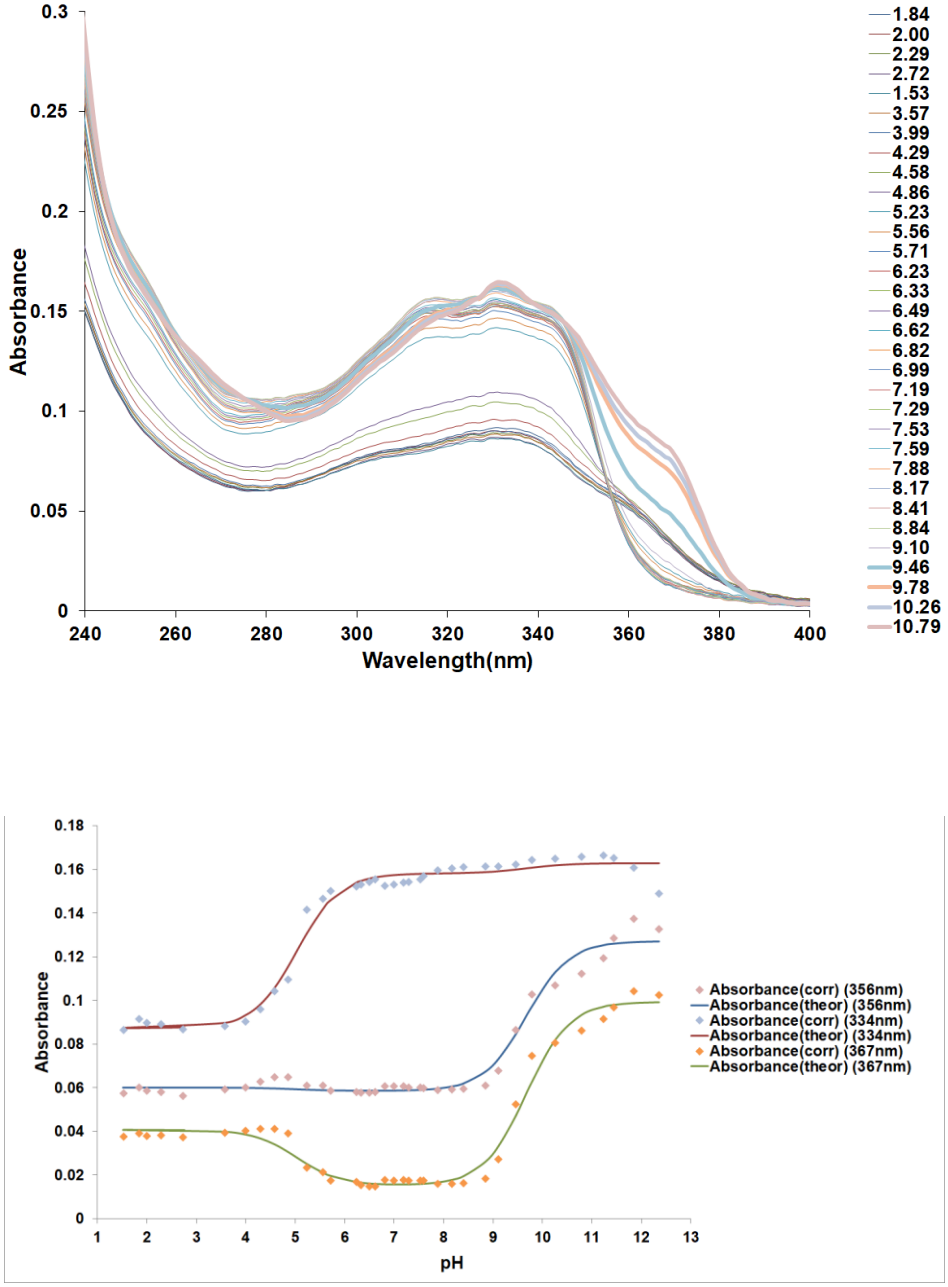

Figure A-5: (Top) Spectra of BIP ($2x10^{-5}$ M) titrated in aqueous solution and 0.0 M ionic strength at ~25°C. (Bottom) Variation of absorbance at three different wavelengths of $2x10^{-5}$ M BIP in aqueous solution as a function of pH. The points are experimental values, whereas the solid lines are theoretical curves fitted to the experimental data using Solver. This titration was done with a comparable solution in the reference cell. (Std Dev: 356nm = ±0.0019, 334nm = ±0.0013, 367nm = ±0.0046)

Table A-2: BIP pK_a values at ~25°C. The pK_a values were obtained at 0.0 M ionic strength.

Dissociation reaction	Dissociation Constant	
$H_2A^+ \rightarrow HA + H^+$	5.04 ± 1.0	pK_{a1}
$HA \rightarrow A^- + H^+$	9.67 ± 1.9	pK_{a2}

Compound #2 Data and Results

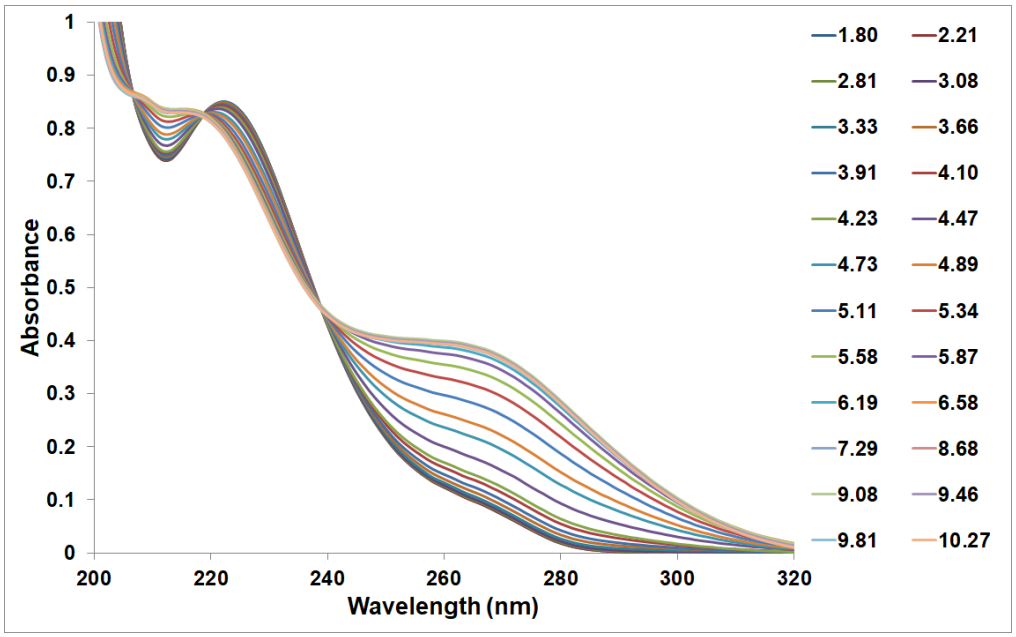

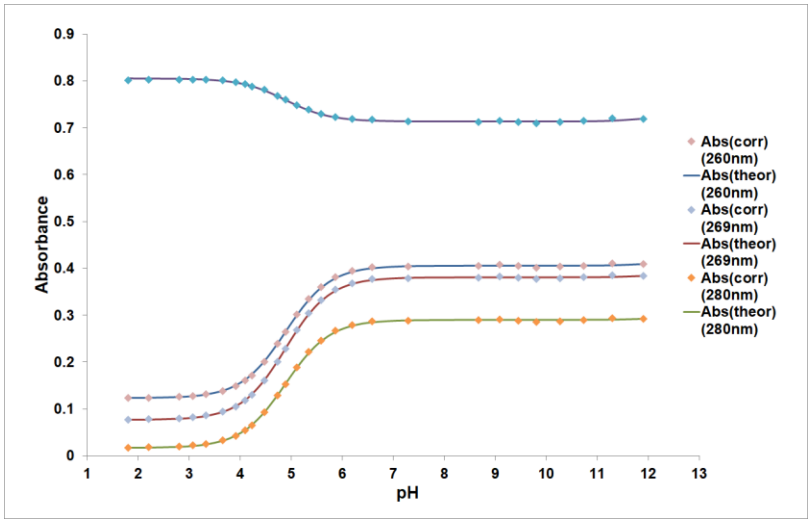

Figure A-6: (Top) Spectra of IP#2 ($8x10^{-5}$ M) in aqueous solution and 0.0 M ionic strength at ~25°C. (Bottom) Variation of absorbance at two different wavelengths of $8x10^{-5}$ M IP#2 in aqueous solution as a function of pH. The points are experimental values, whereas the solid lines are theoretical curves fitted to the experimental data using Solver. This titration was done with a comparable solution in the reference cell. (Std Dev: 260nm = ±0.0017, 269nm = ±0.0017, 280nm = ±0.0017)

Table A-3: Compound #2 pK_a values at ~25°C. The pK_a values were obtained at 0.0 M ionic strength.

Dissociation reaction	Dissociation Constant	
$H_2A^+ \rightarrow HA + H^+$	4.89 ± 0.01	pK_{a1}
$HA \rightarrow A^- + H^+$	13.22 ± 0.1	pK_{a2}

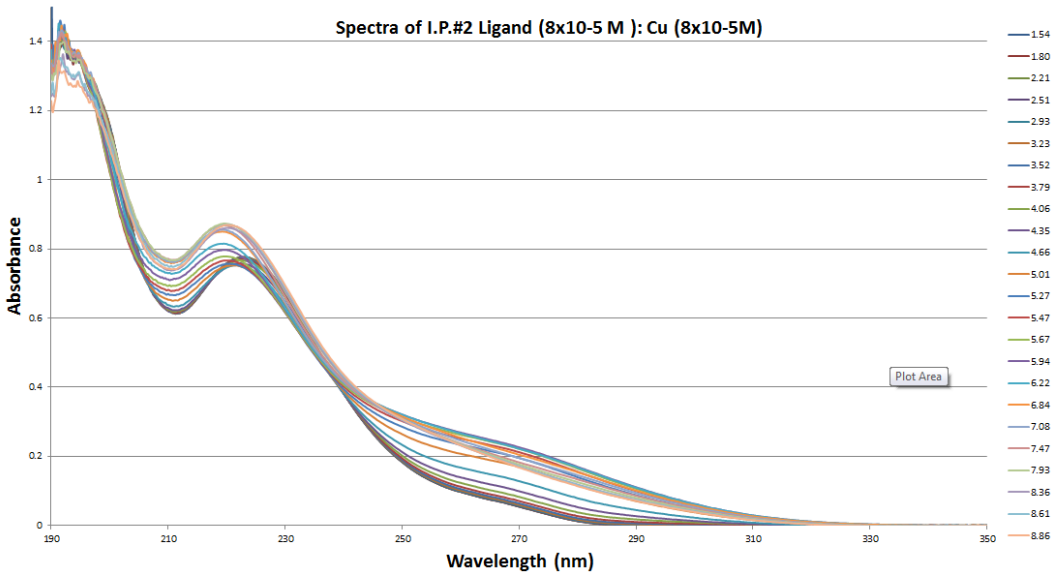

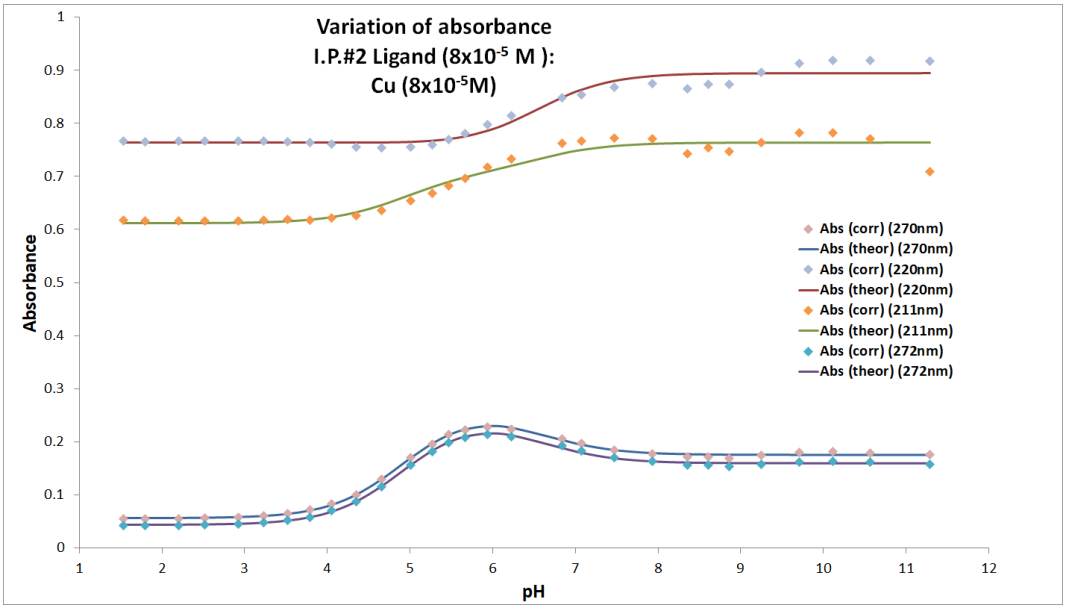

Figure A-7: (Top) Spectra of IP#2 ($8x10^{-5}$ M) titrated at a 1 to 1 ratio with Cu^{2+} (copper(II) sulfate anhydrous) in aqueous solution and 0.0 M ionic strength at ~25°C. (Bottom) Variation of absorbance at four different wavelengths of $8x10^{-5}$ M IP#2 in aqueous solution as a function of pH. The points are experimental values, whereas the solid lines are theoretical curves fitted to the experimental data using Solver. This titration was done with a comparable solution in the reference cell. (Std Dev: 270nm = ±0.0025, 220nm = ±0.013, 211nm = ±0.015, 272nm = ±0.0024)

Table A-4: Compound #2 titrated with Cu^{2+} (copper(II) sulfate anhydrous) pK_a values at ~25°C. The pK_a values were obtained at 0.0 M ionic strength.

Dissociation reaction	Dissociation Constant	
$H_2A^+ \rightarrow HA + H^+$	4.91 ± 0.05	pK_{a1}
$HA \rightarrow A^- + H^+$	6.56 ± 0.3	pK_{a2}

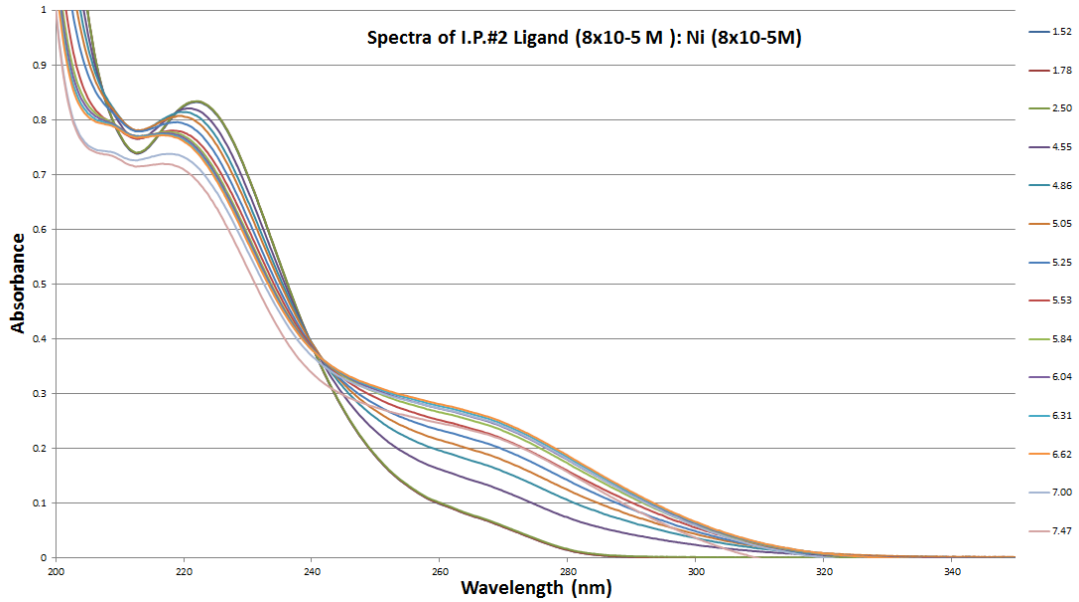

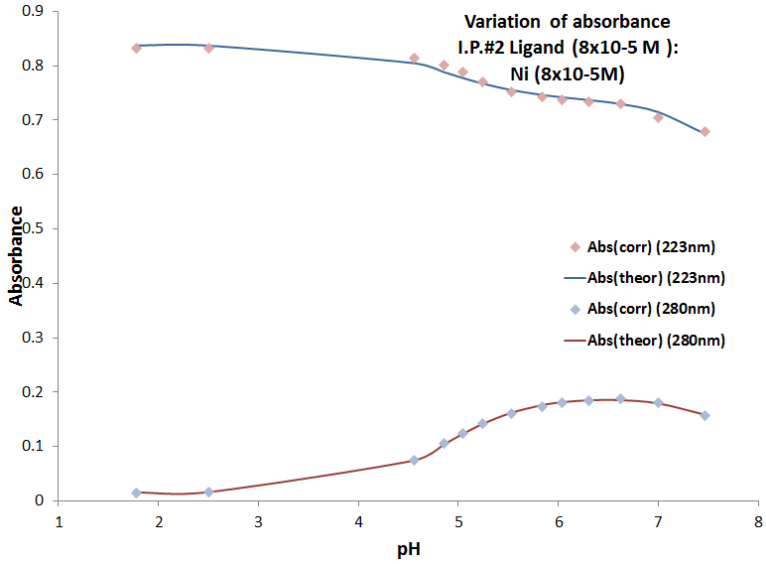

Figure A-8: (Top) Spectra of IP#2 ($8x10^{-5}$ M) titrated at a 1 to 1 ratio with Ni^{2+} (nickel nitrate hexahydrate) in aqueous solution and 0.0 M ionic strength at ~25°C. (Bottom) Variation of absorbance at two different wavelengths of $8x10^{-5}$ M IP#2 as a function of pH. The points are experimental values, whereas the solid lines are theoretical curves fitted to the experimental data using Solver. This titration was done with a comparable solution in the reference cell. (Std Dev: 223nm = ±0.0068, 280nm = ±0.0016)

Table A-5: Compound #2 titrated with Ni^{2+} (nickel nitrate hexahydrate) pK_a values at ~25°C. The pK_a values were obtained at 0.0 M ionic strength.

Dissociation reaction	Dissociation Constant	
$H_2A^+ \rightarrow HA + H^+$	4.86 ± 0.0	pK_{a1}
$HA \rightarrow A^- + H^+$	8.12 ± 0.0	pK_{a2}

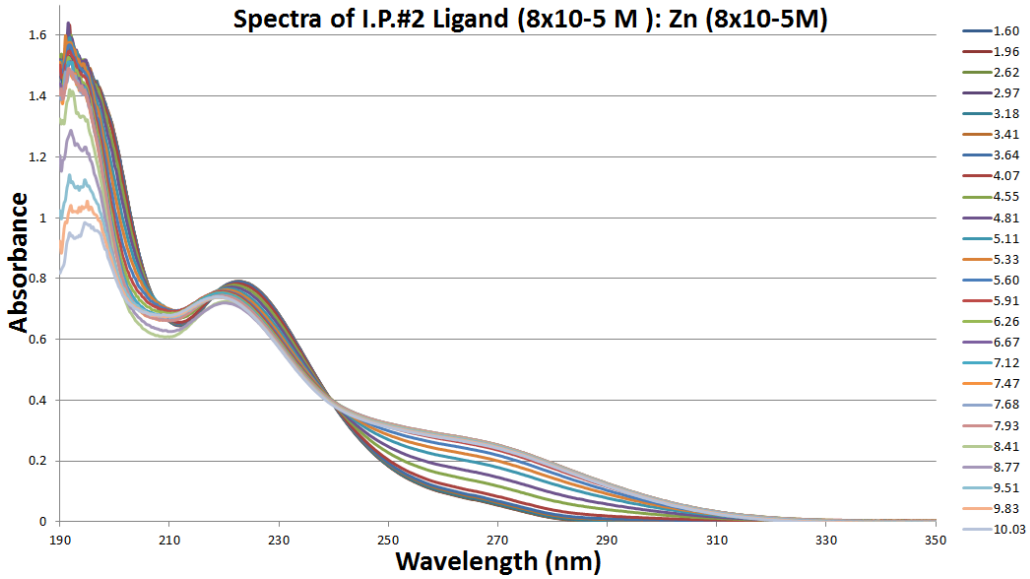

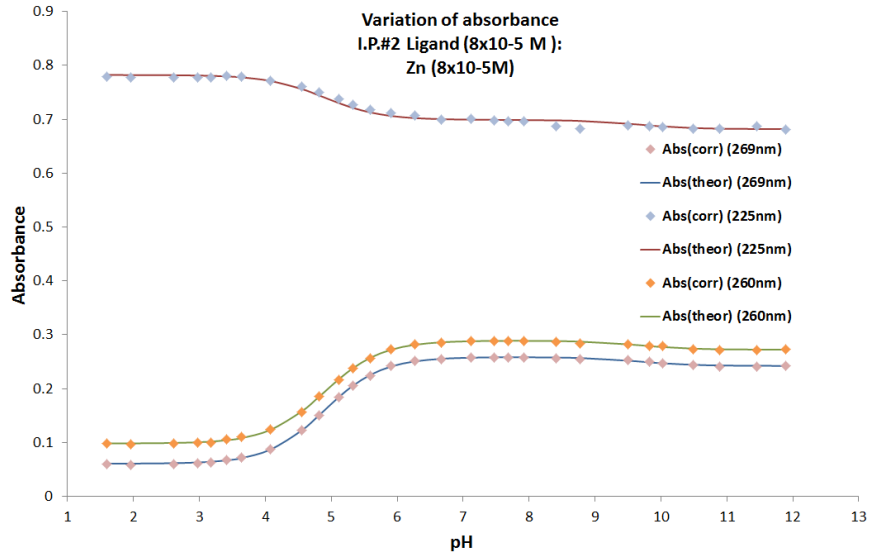

Figure A-9: (Top) Spectra of IP#2 ($8x10^{-5}$ M) titrated at a 1 to 1 ratio with Zn^{2+} (zinc nitrate hexahydrate) in aqueous solution and 0.0 M ionic strength at ~25°C. (Bottom) Variation of absorbance at three different wavelengths of $8x10^{-5}$ M IP#2 in aqueous solution as a function of pH. The points are experimental values, whereas the solid lines are theoretical curves fitted to the experimental data using Solver. This titration was done with a comparable solution in the reference cell. (Std Dev: 269nm = ±0.0018, 225nm = ±0.0031, 260nm = ±0.0018)

Table A-6: Compound #2 titrated with Zn^{2+} (zinc nitrate hexahydrate) pK_a values at ~25°C. The pK_a values were obtained at 0.0 M ionic strength.

Dissociation reaction	Dissociation Constant	
$H_2A^+ \rightarrow HA + H^+$	4.89 ± 0.02	pK_{a1}
$HA \rightarrow A^- + H^+$	9.66 ± 0.04	pK_{a2}

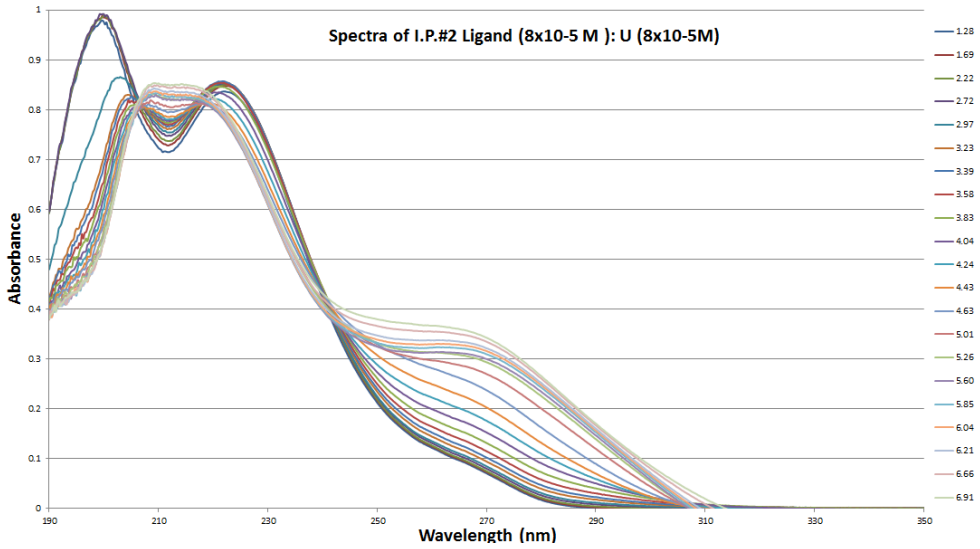

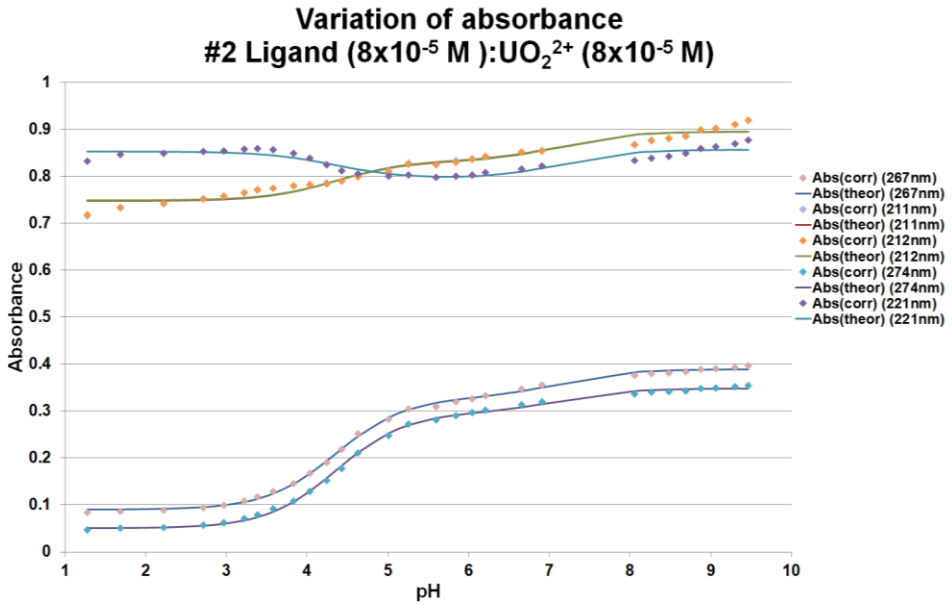

Figure A-10: (Top) Spectra of IP#2 ($8x10^{-5}$ M) titrated at a 1 to 1 ratio with UO_2^{2+} (uranyl nitrate) in aqueous solution and 0.0 M ionic strength at ~25°C. (Bottom) Variation of absorbance at three different wavelengths of $8x10^{-5}$ M IP#2 in aqueous solution as a function of pH. The points are experimental values, whereas the solid lines are theoretical curves fitted to the experimental data using Solver. This titration was done with a comparable solution in the reference cell. (Std Dev: 267nm = ±0.0040, 211nm = ±0.012, 212nm = ±0.012, 274nm = ±0.0038, 221nm = ±0.0093)

Table A-7: Compound #2 titrated with UO_2^{2+} (uranyl nitrate) pK_a values at ~25°C. The pK_a values were obtained at 0.0 M ionic strength.

Dissociation reaction	Dissociation Constant	
$H_2A^+ \rightarrow HA + H^+$	4.36 ± 0.4	pK_{a1}
$HA \rightarrow A^- + H^+$	7.15 ± 0.4	pK_{a2}

Table A-8: Compound #2 pK_{a2} and log(K) values for titrations done with comparable reference solutions.

Ion	**pK_{a2}**	**log(K)**
Cu^{2+}	6.56 ± 0.3	11.06 ± 0.4
UO_2^{2+}	7.15 ± 0.4	10.47 ± 0.5
Ni^{2+}	8.12 ± 0.0	9.49 ± 0.01
Zn^{2+}	9.66 ± 0.04	8.00 ± 0.05

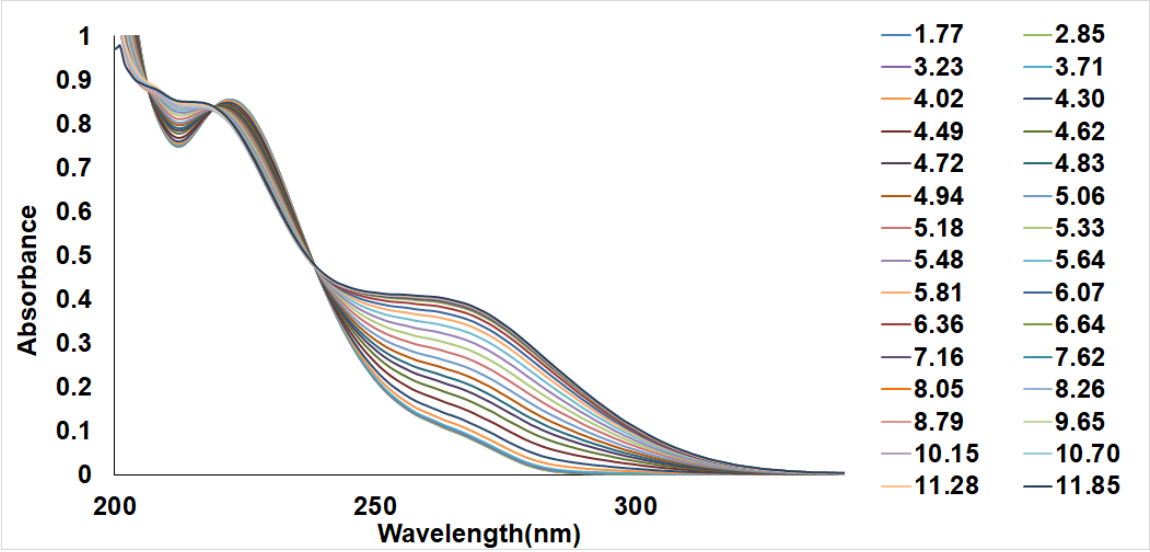

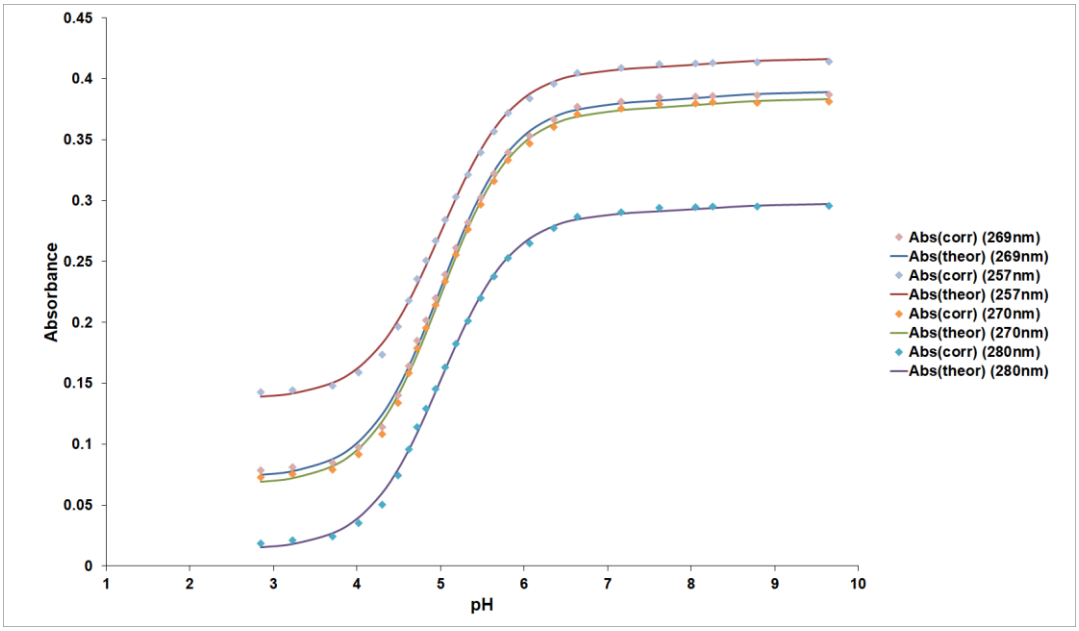

Figure A-11: (Top) Spectra of IP#2 ($8x10^{-5}$ M) titrated at a 1 to 1 ratio with Zn^{2+} (zinc perchlorate hexahydrate) in aqueous solution and 0.0 M ionic strength at ~25°C. (Bottom) Variation of absorbance at four different wavelengths of $8x10^{-5}$ M IP#2 as a function of pH. The points are experimental values, whereas the solid lines are theoretical curves fitted to the experimental data using Solver. This titration was done with DI water only in the reference cell. (Std Dev: 269nm = ±0.0034, 257nm = ±0.0031, 270nm = ±0.0034, 280nm = ±0.0030).

Table A-9: Compound #2 titrated with Zn^{2+} (zinc perchlorate hexahydrate) pK_a values at ~25°C. The pK_a values were obtained at 0.0 M ionic strength.

Dissociation reaction	Dissociation Constant	
$H_2A^+ \rightarrow HA + H^+$	5.00 ± 0.08	pK_{a1}
$HA \rightarrow A^- + H^+$	8.26 ± 0.05	pK_{a2}

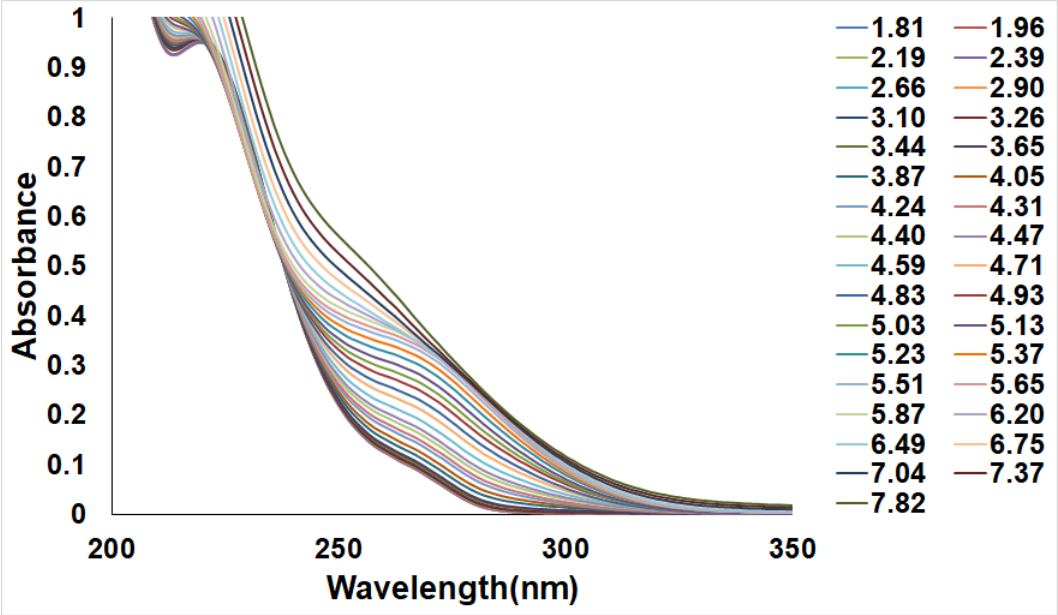

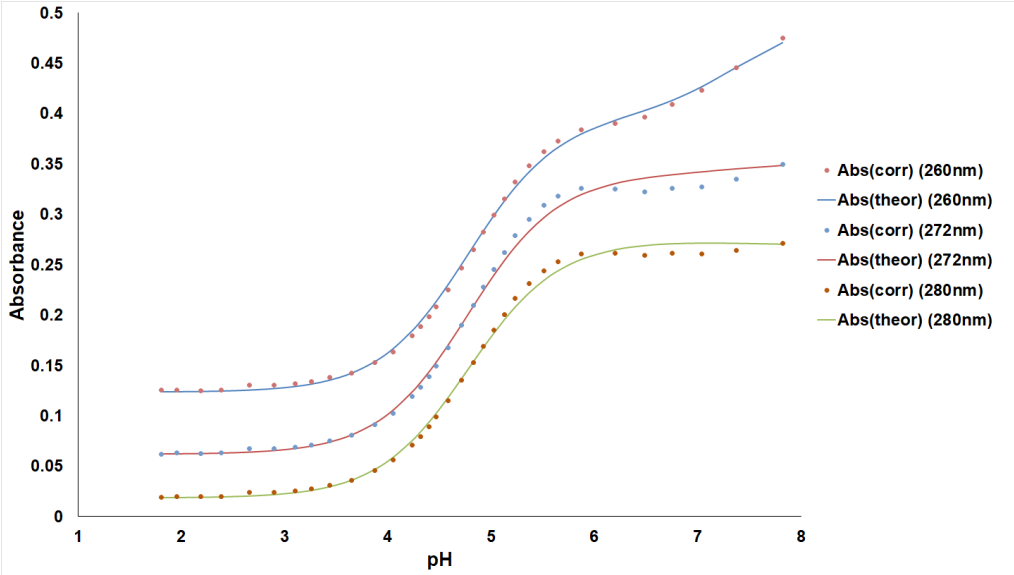

Figure A-12: (Top) Spectra of IP#2 ($8x10^{-5}$ M) titrated at a 1 to 1 ratio with Cu^{2+} (copper(II) perchlorate hexahydrate) in aqueous solution and 0.0 M ionic strength at ~25°C. (Bottom) Variation of absorbance at four different wavelengths of $8x10^{-5}$ M IP#2 as a function of pH. The points are experimental values, whereas the solid lines are theoretical curves fitted to the experimental data using Solver. This titration was done with DI water only in the reference cell. (Std Dev: 260nm = ±0.0053, 272nm = ±0.0065, 280nm = ±0.0050).

Table A-10: Compound #2 titrated with Cu^{2+} (copper(II) perchlorate hexahydrate) pK_a values at ~25°C. The pK_a values were obtained at 0.0 M ionic strength.

Dissociation reaction	Dissociation Constant	
$H_2A^+ \rightarrow HA + H^+$	4.39 ± 0.07	pK_{a1}
$HA \rightarrow A^- + H^+$	7.39 ± 0.4	pK_{a2}

Table A-11: Compound #2 pK_{a2} and log(K) values for titrations done with DI water as the reference.

Ion	**pK_{a2}**	**log(K)**
Cu^{2+}	7.39 ± 0.4	10.22 ± 0.5
Zn^{2+}	8.26 ± 0.05	9.40 ± 0.06

Compound #3 Data and Results

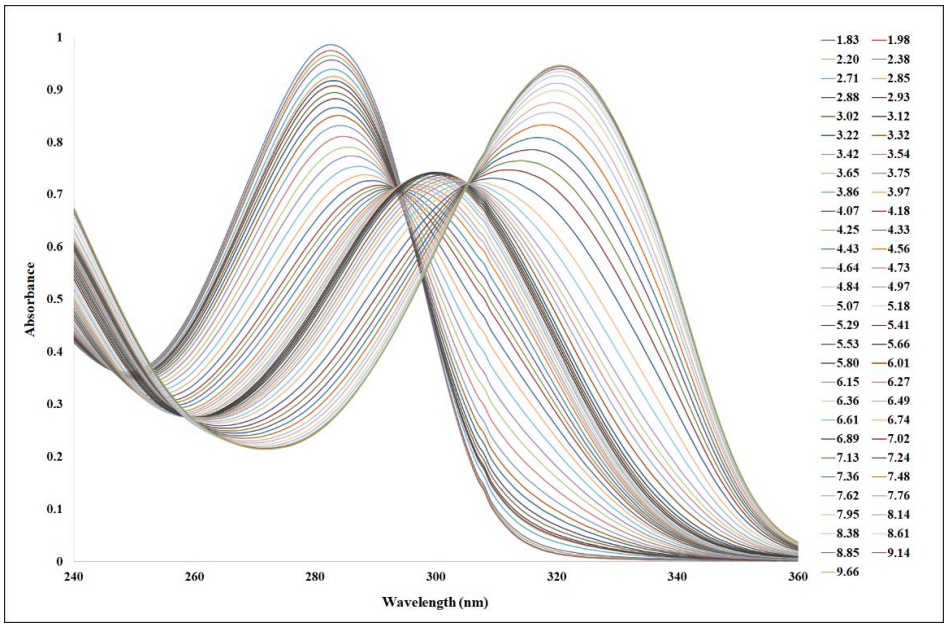

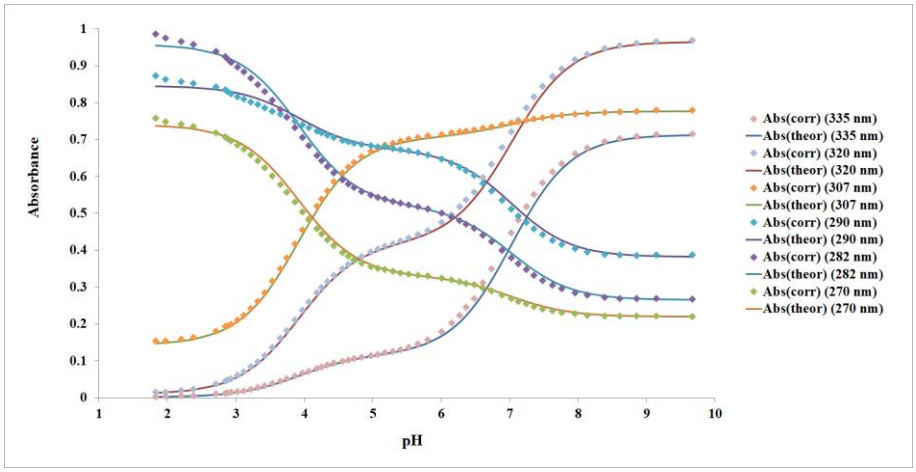

Figure A-13: (Top) Spectra of IP#3 ($7x10^{-5}$ M) in aqueous solution and 0.0 M ionic strength. (Bottom) Variation of absorbance at six different wavelengths of $7x10^{-5}$ M IP#3 as a function of pH. The points are experimental values, whereas the solid lines are theoretical curves fitted to the experimental data using Solver. This titration was done under N_2 purge and agitation, with temperature control at 25°C, and the reference cell had DI water only. (Std Dev: 335nm = ±0.013, 320nm = ±0.013, 307nm = ±0.0067, 290nm = ±0.011, 282nm = ±0.013, 270nm = ±0.0095).

Table A-12: Compound #3 pK_a values at ~25°C. The pK_a values were obtained at 0.0 M ionic strength and the pK_{a2} was obtained at 0.02 M ionic strength.

Dissociation reaction	Dissociation Constant	
$H_2A^+ \rightarrow HA + H^+$	3.92 ± 0.08	pK_{a1}
$HA \rightarrow A^- + H^+$	7.02 ± 0.02	pK_{a2}

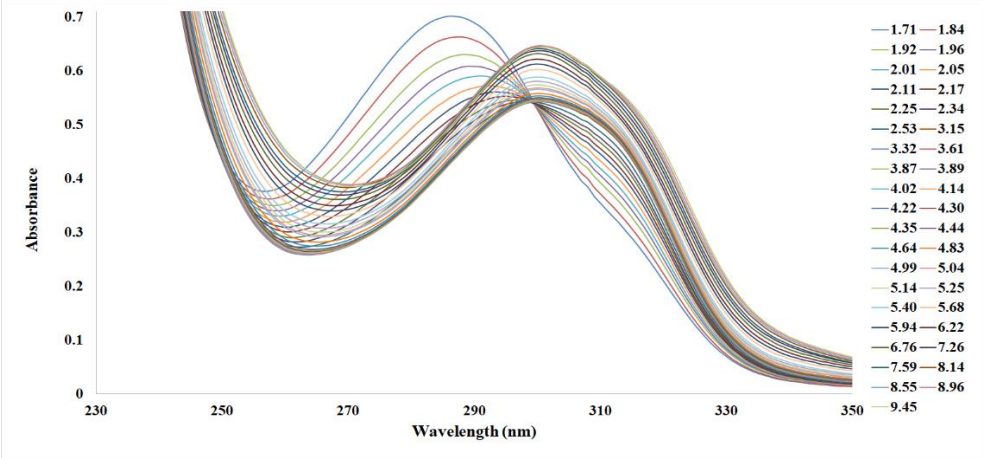

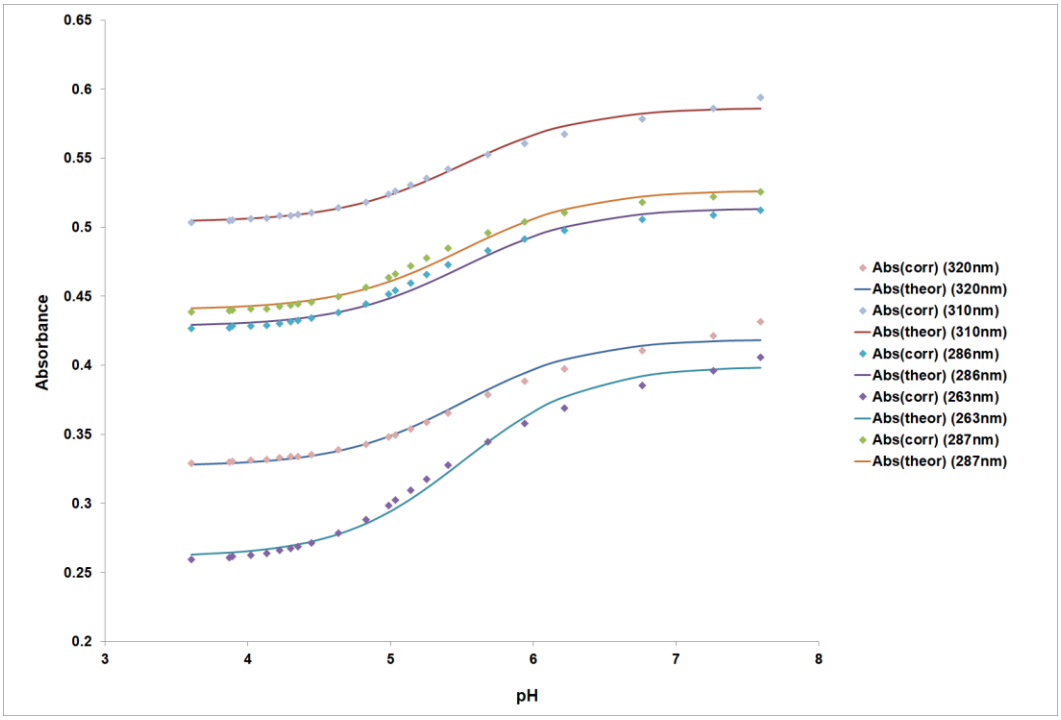

Figure A-14: (Top) Spectra of IP#3 ($7x10^{-5}$ M) in aqueous solution titrated at a 1 to 1 ratio with UO_2^{2+} (Uranyl nitrate) and 0.0 M ionic strength. (Bottom) Variation of absorbance at five different wavelengths of $7x10^{-5}$ M IP#3 and with UO_2^{2+} as a function of pH. The points are experimental values, whereas the solid lines are theoretical curves fitted to the experimental data using Solver. This titration was done under N_2 purge and agitation, with temperature control at 25°C, and the reference cell had DI water only. (Std Dev: 320nm = ±0.0038, 310nm = ±0.0025, 280nm = ±0.0033, 263nm = ±0.0044, 287nm = ±0.0032).

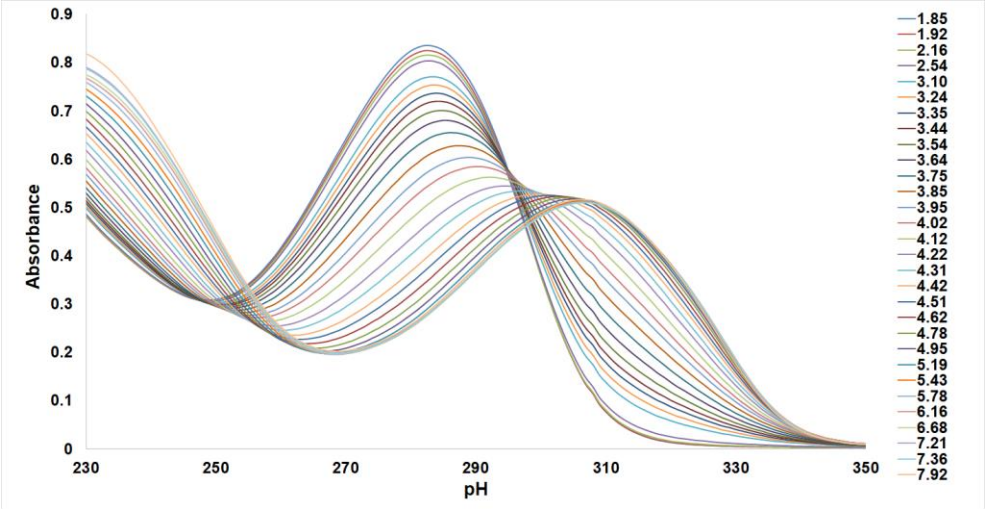

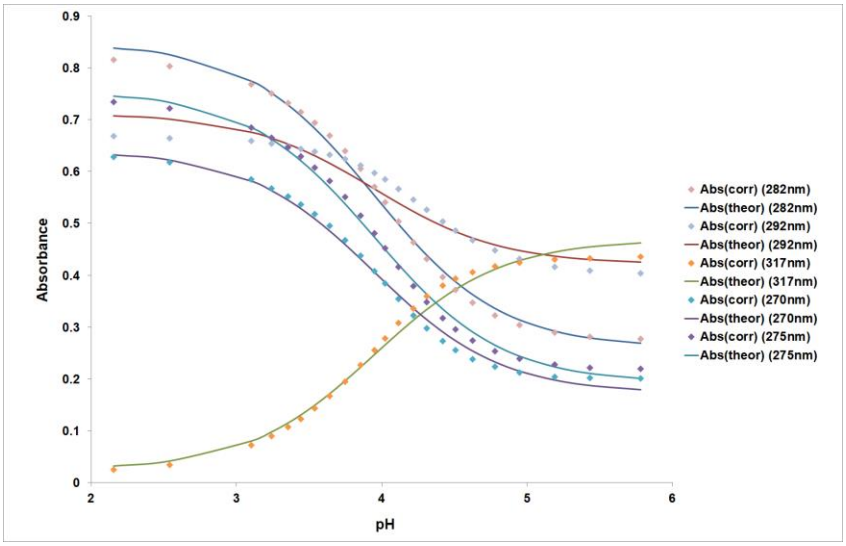

Figure A-15: (Top) Spectra of IP#3 ($7x10^{-5}$ M) in aqueous solution titrated at a 1 to 1 ratio with Zn^{2+} (zinc perchlorate hexahydrate) and 0.0 M ionic strength. (Bottom) Variation of absorbance at five different wavelengths of $7x10^{-5}$ M IP#3 and with Zn^{2+} as a function of pH. The points are experimental values, whereas the solid lines are theoretical curves fitted to the experimental data using Solver. This titration was done under N_2 purge and agitation, with temperature control at 25°C, and the reference cell had DI water only. (Std Dev: 282nm = ±0.013, 292nm = ±0.021, 317nm = ±0.015, 270nm = ±0.012, 275nm = ±0.012)

Table A-13: Compound #3 with Metals (uranyl nitrate and zinc perchlorate hexahydrate) pK_a and log(K) values at 25°C. The pK_a value was obtained at 0.0 M ionic strength.

Dissociation reaction	Dissociation Constant	
Dissociation Constant (pK_{a1})	log(K)	Metal Species
5.25 ± 0.2	6.23 ± 0.2	UO_2^{2+}
4.05 ± 0.09	7.43 ± 0.1	Zn^{2+}

VITA

KC Mote attended high school in Alaska, after she graduated, she worked while attending college at the University of Alaska Southeast before moving to Tennessee and attending Volunteer State Community college, where she earned her Associates of Science degree. Afterwards, she transferred to Tennessee Technological University where she worked as a teaching assistant and earned her Bachelor of Arts and Science degree. She then attended the University of Tennessee where she was a teaching assistant and worked in the laboratory titrating small molecules for the study of amidoximated polymers and their adsorption of uranium from seawater.